

# The electrophysiology of the $\beta$ -cell based on single transmembrane protein characteristics

**Michael E. Meyer-Hermann**

Frankfurt Institute for Advanced Studies (FIAS),  
Max von Laue Str. 1, 60438 Frankfurt/Main, Germany  
Email: M.Meyer-Hermann@fias.uni-frankfurt.de  
phone: +49 69 798 47508; fax +49 69 798 47611

## **Keywords:**

electrical bursting, insulin secretion, calcium dynamics,  
ion-channels, ATPases, mathematical modelling

## **Abstract:**

The electrophysiology of  $\beta$ -cells is at the origin of insulin secretion.  $\beta$ -cells exhibit a complex behaviour upon stimulation with glucose including repeated and uninterrupted bursting. Mathematical modelling is most suitable to improve knowledge about the function of various transmembrane currents provided the model is based on reliable data. This is the first attempt to build a mathematical model for the  $\beta$ -cell-electrophysiology in a bottom-up approach which relies on single protein conductivity data. The results of previous whole-cell-based models are reconsidered. The full simulation including all prominent transmembrane proteins in  $\beta$ -cells is used to provide a functional interpretation of their role in  $\beta$ -cell-bursting and an updated vantage point of  $\beta$ -cell-electrophysiology. As a result of a number of *in silico* knock-out- and block-experiments the novel model makes some unexpected predictions: Single-channel conductivity data imply that calcium-gated potassium currents are rather small. Thus, their role in burst interruption has to be revisited. An alternative role in high calcium level oscillations is proposed and an alternative burst interruption model is presented. It also turns out that sodium currents are more relevant than expected so far. Experiments are proposed to verify these predictions.

# 1 Introduction

The electrophysiology of  $\beta$ -cells is most relevant for understanding possible regulatory targets of insulin secretion. Exocytosis of insulin loaded granules is, among others, governed by intracellular calcium signalling. Calcium dynamics exhibits very specific patterns in reaction to increased glucose concentrations which includes repeated bursting of the membrane potential. Bursting denotes oscillations of action potential-like depolarisations, which are regularly interrupted and set in again after a phase of silence. Thus, oscillations occur on two distinct time scales: Fast oscillation of the membrane potential on the scale of 100 milliseconds and slow oscillations of intracellular calcium on the time scale of 10 seconds, i.e. in the rhythm of the repetition of bursting events.

In a minimal model of oscillations of the membrane potential (1) it was found that an activation-delay between voltage-gated potassium and calcium channels gives rise to this bursting behaviour. Sodium, the major player in neurons, is generally believed to be of minor importance (2). Therefore, modelling work was concentrating on potassium and calcium currents (3–5).

Initiation of bursting events was found to be related to ATP-driven potassium channels (6, 7) which induce a relevant outflow of potassium under resting conditions. When glucose – and via glucose metabolism – ATP is increased, the channel conductivity is inhibited (8, 9), which leads to the initial depolarisation. Then voltage-dependent calcium currents are activated and the delayed response of voltage-dependent potassium currents leads to the bursting event.

Simulations of the  $\beta$ -cell-electrophysiology have shown how, in principle, repeated bursting can happen (1–3, 5). And the found mechanisms are in agreement with experimental results. However, none of the presently existing models fulfill the following requirements: (i) All important ions and membrane proteins are explicitly modeled including their activation and inactivation dynamics; (ii) the  $\beta$ -cell exhibits a steady state and is stimulated by changes of glucose concentrations; (iii) the dynamics of the membrane protein activity are fully derived from protein experiment. Only if all these requirements are respected, the exact role of the different membrane proteins might be disentangled.

A major problem in developing such a complete simulation tool is related to the large variety of measured whole-cell conductivities in  $\beta$ -cells. In fact the density of the membrane proteins is itself a dynamical quantity. Their dynamics vary for different cell-types so that the data used for modelling are restricted to measurements in  $\beta$ -cells. Not all membrane proteins have been subject to quantitative measurements in  $\beta$ -cells and the  $\beta$ -cells under consideration can be in various states of protein expression. Thus, modelling work was restricted to fit the activity-dynamics of the membrane proteins to the behaviour which was expected.

In order to overcome this problem, the present simulation exclusively relies on data of single protein activity. Such an approach was used in calcium modelling of neurons (10) before and is now applied for the first time to  $\beta$ -cell electrophysiology. Today there is a rather complete knowledge about single proteins conductivity and opening dynamics available which allows a bottom-up approach starting from the single protein level.

To this end the single protein activity dynamics is separated from the protein density. It is assumed that the single protein dynamics is cell-independent. In other words a voltage-gated

potassium channel has the same dynamical properties in a neuron and in a  $\beta$ -cell. This assumption might be set in question if cooperation of membrane proteins with other cell structures would change the activity dynamics. However, the universality of single membrane protein properties can be considered to be a good approximation because the measured characteristics of the cells show relatively small variations despite them stemming from different cell-types.

The conductivity and opening properties of single proteins are exactly implemented into the model and then are multiplied by the surface density of the respective proteins in  $\beta$ -cells. The latter are not precisely known and are the free parameters of the simulation. In comparison to the huge parameter space in simulations relying on whole-cell conductivity measurements, this is a rather small set of unknown parameters. This improves the predictive power of the mathematical model. The behaviour of the  $\beta$ -cell in terms of dynamics of membrane potential and ion-concentrations is emerging from the single protein level, thus, coupling the molecular to the cellular level.

The framework of the simulation is presented in the methods section. The single membrane protein properties are collected in the supplementary material. These define the current dynamics as used in the simulation. The full model as introduced in Section 2 contains the model of a most prominent original work (3). The bursting behaviour as found in Sherman et al's work is reproduced as a special case of the full model and is used as test for the simulation. Then the full simulation is employed to set up a steady state of the  $\beta$ -cell, and to allow for stimulation of the  $\beta$ -cell with glucose. The protein densities are determined to find a realistic behaviour of the cell – where the single membrane protein properties are not touched. On the basis of this simulation various *in silico* experiments are performed and compared to real experiments if available.

The *in silico* experiments include knock-out experiments and partial or total block of membrane proteins. Calcium-driven potassium channels are modeled according to data that are used for  $\beta$ -cell-simulations for the first time. The measured dynamics leads to the conclusion that this channel is of minor importance at normal glucose levels, while it is most important for the  $\beta$ -cell-behaviour at supra-large glucose levels. In this regime calcium-driven potassium channels drive uninterrupted bursting (7). LVA-channels, which have not been considered in other models, NCX, and PMCA are suggested to be important for the interruption of bursting events at normal glucose levels. Also the importance of a dynamic reversal potential, which was mostly neglected in other work, is pointed out. It is found that the role of sodium currents was underestimated so far, and their impact on  $\beta$ -cell behaviour is explained. The paper is concluded with a novel vantage point on the interplay of the different ion-conducting membrane proteins during repeated and uninterrupted bursting. Novel experiments are suggested to verify the new vantage point.

## 2 Methods

### 2.1 Dynamics of ion concentrations and membrane potential

Rate equations are used to describe the dynamics of intracellular ion concentrations. External ion concentrations are assumed constant. The ions treated explicitly are sodium  $N$ , potassium  $K$  and calcium  $C$ . The dynamics depends on the conductivity of various membrane proteins which each correspond to one term in the following differential equations.

$$\begin{aligned}
 \frac{dN}{dt} &= -\frac{\xi}{F} (\rho_{Na,V} I_{Na,V} + 2\rho_{Na,K} I_{Na,K} \alpha_{Na,K} + \rho_{NCX} I_{NCX} \alpha_{NCX} + J_{Na}) \\
 \frac{dK}{dt} &= -\frac{\xi}{F} \left( \rho_{K,ATP} I_{K,ATP} + \rho_{K,V} I_{K,V} + \rho_{K,Ca} I_{K,Ca} - \frac{4}{3} \alpha_{Na,K} \rho_{Na,K} I_{Na,K} + J_K \right) \\
 \frac{dC}{dt} &= -\frac{\xi}{z_{Ca} F (1 + x_c)} \left( \rho_{Ca,L} I_{Ca,L} + \rho_{Ca,T} I_{Ca,T} - \frac{1}{3} z_{Ca} \alpha_{NCX} \rho_{NCX} I_{NCX} \right. \\
 &\quad \left. + \rho_{PMCA} I_{PMCA} + J_{Ca} \right) .
 \end{aligned} \tag{1}$$

$I_x$  denote the electrical single membrane protein currents, where  $x$  specifies the type of membrane protein as defined in Figure 1 (see also Tab. 1 in the supplement). Negative currents are defined to bring positive ions (charges) into the cell. As the currents are not defined as ion currents but as electrical currents they have to be weighted by factors denoting the valence of the ion  $z_{Ca} = 2$  and the stoichiometry of the protein  $\alpha_x$ . The single membrane protein currents and their dynamics are discussed in the supplementary material Section 5.1 and are schematically visualised in Figure 1.

$\rho_x$  denote the corresponding surface densities of the membrane proteins.  $\xi = 3$  is a surface to volume factor that relates the current through the membrane to a change of the ion concentration in the intracellular volume. The cell geometry is assumed to be approximately spherical which implies  $\xi = 3/r$  where  $r$  is the cell radius.

Note that a calcium buffer is included in the equation for calcium. The calcium buffer is assumed to bind and dissolve calcium faster than the typical time scale of the ion dynamics. Thus, the kinetic equation for the buffer can be solved in the steady state approximation (rapid buffer approximation). This implies an additional factor  $(1 + x_c)$  in the equation for calcium, where

$$x_c = \frac{c_0 K_c}{(C + K_c)^2} , \tag{2}$$

with  $c_0$  the total concentrations of the buffering calcium binding sites. The most prominent buffer is calmodulin having more than one calcium binding site.  $K_c$  is the dissociation constant of the calcium binding sites.  $C$  is the free calcium concentration. The total calcium concentration is given by

$$C_{total} = C \left( 1 + \frac{c_0}{C + K_c} \right) . \tag{3}$$

The fraction of free calcium is  $f_{Ca} = \frac{C}{C_{total}}$  and adopts values between 0.1 and 1%.

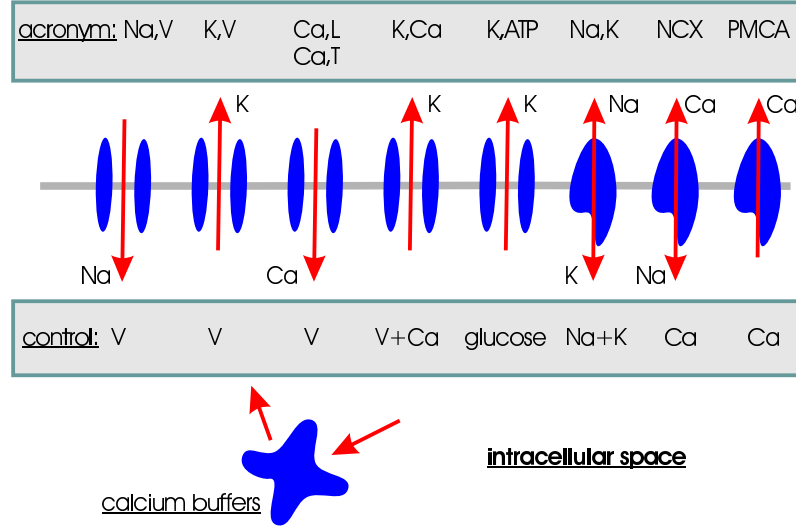


Figure 1: **Schematic representation of ion-conducting transmembrane proteins:** The plasma membrane is visualised as horizontal grey line on which a set of transmembrane proteins are shown. The shaded boxes show the *acronyms* of the proteins and the quantities that *control* their gating/activity in the model introduced below. The ions attributed to the arrows denote the direction of ion flow (assuming normal electrochemical gradients). The *calcium buffers* symbolise all kinds of intracellular calcium binding sites, including calmodulin and organelles acting as calcium stores. The acronyms of the membrane proteins are also defined in Tab. 1 in the supplement, where also the activity dynamics are explained in detail.

$J_{K,Na,Ca}$  denote the leakage currents. They are derived from the steady state limit (see Eq. 24 in the supplement) to guarantee a resting state of the cell. In the resting state all other currents are balanced by the leakage currents, so that the net current vanishes and the ion concentrations are constant.

The ions build up the membrane potential  $V$ . All non-electroneutral currents introduced in Eq. 1 show up in the equation for  $V$ :

$$\begin{aligned} \frac{dV}{dt} = & -\frac{1}{C_m} (\rho_{Na,K} I_{Na,K} + \rho_{K,ATP} I_{K,ATP} + \rho_{K,V} I_{K,V} + \rho_{K,Ca} I_{K,Ca} + \rho_{Na,V} I_{Na,V} \\ & + \rho_{NCX} I_{NCX} + \rho_{PMCA} I_{PMCA} + \rho_{Ca,L} I_{Ca,L} + \rho_{Ca,T} I_{Ca,T} \\ & + J_K + J_{Na} + J_{Ca}) \quad . \end{aligned} \quad (4)$$

No additional leakage current is needed because in the steady state the right hand side vanishes by construction.  $C_m$  is the membrane capacitance that relates the electrical currents to changes of the membrane potential.

## 2.2 Reversal potentials

Reversal potentials depend on the chemical gradient and the membrane potential over the cellular membrane. They cannot be considered to be constant (as assumed in most other models). As the reversal potentials linearly enter Ohm's law (which is used to approximate ion current through open pores) this has to be accounted for. The Nernst-equation is used to calculate the correct reversal potential during dynamical changes of the electrochemical constellation:

$$\overline{V}_x = \frac{RT}{z_x F} \ln \left( \frac{x_{\text{ext}}}{x} \right) \quad , \quad (5)$$

where  $x = \text{K, Na, Ca}$ , and  $R = 8.315 \text{ J/(K mol)}$  the Rydberg (molar) gas constant. The temperature  $T$  is assumed to be the physiological temperature.  $x_{\text{ext}}$  is the external concentration of the ion (in thermic bath approximation). They are calculated from the intracellular ion-concentrations at rest state to fit the known reversal potential  $V_{\text{K}} = -75 \text{ mV}$ ,  $V_{\text{Na}} = +80 \text{ mV}$ ,  $V_{\text{Ca}} = +128 \text{ mV}$ .

The straight forward application of Nernst equation, which is based on thermodynamical notions and only involves the electro-chemical gradient of the ion under consideration, thus, neglecting other ions and not treating diffusion of ions correctly, is not always justified. In the case of calcium a more exact theoretical approach based on the Goldman-Hodgkin-Katz equation leads to a non-linear I-V-relationship (see e.g. (11)). This equation is derived from the theory of electro-diffusion through a membrane and involves the influence of other ions on the reversal potential. This more precise I-V-relationship is approximated by an Ohm's law like current, which is only justified for the linear piece of the curve. A good approximation is to use a corrected reversal potential of  $V_{\text{Ca}} = +50 \text{ mV}$ . Up to this rather large membrane potential the I-V-relationship is, indeed, approximately linear. However, one should keep in mind that for depolarisation beyond  $50 \text{ mV}$  (thus of  $\Delta V = 120 \text{ mV}$  relative to the resting potential) the calcium currents are not correctly represented.

## 2.3 The basic model assumptions

The following list summarises the most important features, assumptions, and limitations of the  $\beta$ -cell-model:

*Universality of single membrane protein measurements:*

It is assumed that the measured single membrane protein conductivities and opening dynamics are valid irrespective of the cell-type. This considerably increases the data basis of the simulation. In view of consistent measurements of the same protein in different cells this approximation is reasonable. These parameters are only varied in order to investigate robustness issues.

*Stability of the  $\beta$ -cell-resting state:*

The leakage currents are assumed to equilibrate all other currents if all cell properties are at their resting values. This implies that the cell exhibits a stable steady state and that the cell returns to this resting state after stimulation.

*Glucose- and not ATP-mediated activation:*

Glucose is assumed to directly impact on the conductivity of the K,ATP-channel. Thus, the  $\beta$ -cell can be stimulated by changes of the glucose level. However, the dynamics of ATP (6, 12) which mediates the effect of glucose on K,ATP-channels (13) is not considered and left for future improvements of the simulation. Also any feedback between ATP and calcium is neglected (14).

*Averaging over the whole-cell:*

Inhomogeneities of the cell are averaged out. The ion-concentrations are assumed to be average quantities over the whole-cell.

*Neglect of calcium-induced-calcium-release:*

Calcium-induced-calcium release has been suggested to contribute to the calcium oscillations in response to glucose-induced potassium currents (15). However, blocking of related mechanisms does not affect observed oscillations in pancreatic  $\beta$ -cells (16, 17). Oscillation in the stores might be orchestrated with oscillations in the cytosol (17). The present simulation neglects the effects of calcium-induced-calcium-release and assumes that the endoplasmatic reticulum acts mainly as an additional buffer. Thus, the binding site concentration  $c_0$  is assumed to be larger than expected by calmodulin alone.

*Membrane channels follow Ohm's law:*

The ion flow through an open pore is assumed to follow Ohm's law which implies a linear voltage-current-relation. This is valid for most ion channels. Deviations are found only for extreme membrane potentials which are not considered within this investigation.

*The  $\beta$ -cell is isolated:*

*In vivo*  $\beta$ -cells are in the context of islets and connected with each others by gap-junctions. This connection might influence the susceptibility of stimulation. Indeed,  $\beta$ -cell-stimulation is more difficult in isolated cells (see e.g. (7)). The present simulation neglects effects stemming from being embedded into islets.

## 3 Results

### 3.1 Evaluate the Sherman et al. 1988 model

The model of Sherman et al. (3) can be considered as a classical reference model. It is characterised by the following properties:

- Membrane potential follows a classical ordinary differential equation with capacity 5.31pF and three ionic currents (no leakage and no sodium currents).
- A voltage-gated potassium channel (corresponding to K,V here) is described by a sigmoidal function for its asymptotic value and a differential equation for the opening probability (same as here). Inactivation of K,V-channels is not considered.
- A calcium-gated potassium channel (corresponding to K,Ca here), which is described by a Hill function with Hill coefficient  $n_{K,Ca} = 1$ .



- A calcium channel (corresponding to Ca,L here) including inactivation and fast activation.
- Constant reversal potentials are assumed (no Nernst equation is used).
- The steady state of the system is defined as zero current of the three currents contributing to the voltage equation (thus no leakage currents are considered).
- An equation for calcium ions including two terms and a constant factor  $f = 0.001$  compensating for the buffer (thus, no buffer dynamics). One term accounts for Ca,L-currents the second for calcium removal (corresponding to PMCA here).
- PMCA-activity is not described by a Hill-function but increases linearly with the calcium concentration. Note that in (3) the calcium extrusion term is assumed to be electroneutral, which is not the case as, typically, calcium is removed by PMCA. This pump is not electroneutral. Thus the PMCA-current also enters the equation for the membrane potential Eq. 4 in the present model.

The full model as introduced in Section 2 is reduced to these properties and the results in (3) are reproduced (data not shown). In a second step some parameters are modified to experimentally known values: capacity, resting concentrations, reversal potential of calcium. All these changed values are collected in Tab. 2 – 5 in the supplement. Surprisingly, all modifications together only moderately alter the results (see Figure 2).

The channels in the initial state of the simulation are not equilibrated (thus not in a steady state). This induces a certain inflow of calcium through Ca,L which depolarises the cell. As the K,V current reacts with a delay the potassium outwards current comes later and allows for an above threshold depolarisation. This leads to the oscillation on a higher voltage level. Now, free calcium accumulates in the cell due to repeated inflow. Note that the largest part of the incoming calcium is assumed to bind to the buffer, such that calcium accumulates much slower than according to the calcium inflow. More calcium induces increasing  $g_{K,Ca}$  (note that the K,Ca-currents used in (3) are not in agreement with single protein experiments) and PMCA-activity, which in turn increases the potassium and calcium outflow, respectively. The oscillations are suppressed for some threshold K,Ca and PMCA conductivity. From here the whole process restarts. The essential properties are the delay between Ca,L- and K,V-current, the calcium buffering which induces a slow calcium increase, and a membrane protein which reacts to the increased calcium level by dropping oscillations.

The back-reaction of PMCA activity on the membrane potential was neglected in (3). If this is included into Sherman et al's model, bursting disappears. The back reaction of PMCA activity on the membrane potentials induces hyperpolarisation of the cell. This infers that K,V and K,Ca (in view of the reversal potential of  $\overline{V_K} = -75mV$ ) but more importantly Ca,L (because of very low opening probability) are almost inactive. In this situation PMCA reduces intracellular calcium below its resting state while further hyperpolarising the cell. This is a problem related to lack of steady state in Sherman et al's model. The cell does not go back to resting state after a bursting process. In conclusion, neglect of a back-reaction of the process removing calcium from the cell on the membrane potential turns out not to be a justified approximation.



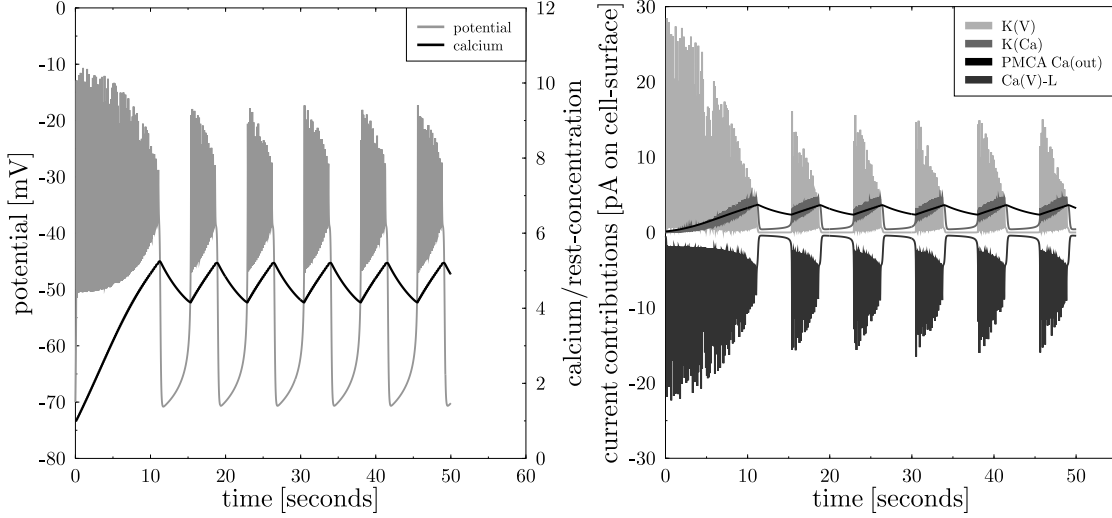
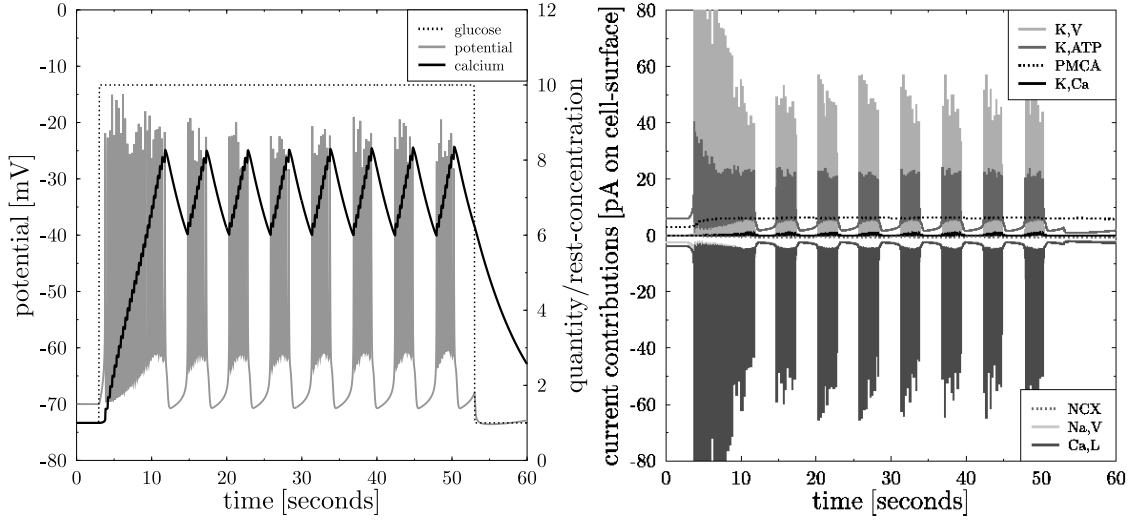


Figure 2: **The simulation is consistent with Sherman et al's model:** A simulation of the model of Sherman et al. (3) with adapted parameters. The membrane potential (left panel, grey line) exhibits repeated bursting events. Intracellular calcium concentration is plotted as ratio to the resting concentration of  $0.1\mu M$  (left panel, black full line). It rises during bursting events and decreases during the silent phase. The contributions of the transmembrane currents are shown in the right panel (the inset lists the currents in the sequence of vertical appearance). Oscillations occur between voltage-gated potassium (K,V right panel, light grey line) and calcium channels (Ca,L right panel, dark grey line). K,Ca- and PMCA-activity follow the calcium level (right panel, medium grey and black line, respectively).

### 3.2 $\beta$ -cell-bursting with calcium, potassium, and sodium currents

The second simulation includes all membrane proteins as introduced in Section 2 and, thus, extends the model (3). The characteristics of activation and inactivation are taken from single protein experiments. The densities are adapted to find reasonable electrical bursting. The resulting set of densities is given in the supplement Tab. 5 (full model). First, the steady state is established and then the cell is stimulated by  $10mM$  glucose. The result is shown in Figure 3 and is in good agreement with corresponding measurements (7, 18). The whole-cell peak ion-currents are  $12$ ,  $50$ , and  $70pA$  for sodium, calcium, potassium, respectively, which is also found in experiments. The whole-cell K,ATP-conductivity is  $1nS$  at  $1mM$  glucose (derived from Figure 4 as  $4\pi r^2 \rho_{K,ATP} \overline{g_{K,ATP}} (1 - g_{K,ATP})$ ), which compares to  $1 - 3nS$  in experiment (19). An analysis of the contributions of the different membrane proteins induces a picture which in parts coincides with the one proposed by Sherman et al. (3). However, there are also some important modifications which will be analysed and isolated in subsequent knock-out and block experiments.



**Figure 3: Repeated bursting including all transmembrane proteins:** The full model for the electrophysiology of the  $\beta$ -cell is used to simulate repeated bursting after activation with glucose. Before stimulation the  $\beta$ -cell exhibits a stable steady state. Activation with  $10mM$  glucose at  $t = 3s$  (left panel, dashed line) first leads to instabilities. Then the membrane potential (left panel, grey line) shows regular repeated bursting activity. The burst to silent ratio and the bursting frequency are realistic. The intracellular calcium level (left panel, black full line) increases and decreases in cycles corresponding to the bursting events. The whole-cell contributions of the different currents are shown in the right panel (the proteins in the inset are given in the sequence of current contributions). Note that here and in the corresponding subsequent figures the electrical currents, not ion-currents, are shown. Therefore the NCX-current appears with negative sign.

### 3.2.1 High resolution of bursting events

A single burst event in Figure 3 is analysed in more detail. To this end a high resolution figure of a burst event is depicted in Figure 5. The analysis is started when the membrane potential has reached its minimum. It can be clearly seen that the burst event is initialised by a K,ATP-current. The Ca,L-current quickly follows. The K,V-currents are suppressed in this phase of the burst event. This is not related to the delayed activation (which causes  $50ms$  at the most) but to the general single protein activation properties. These do not allow for a strong K,V-current near the reversal potential of potassium. K,V-currents become relevant only after strong depolarisations which are induced by strong Ca,L-currents. The delay of K,V-response with respect to the Ca,L-dynamics leads to stable oscillations. Calcium levels increase with each depolarisation spike. This induces small K,Ca-currents, involving a slightly decreasing frequency of spikes during each burst event which is in agreement with experimental data (7, 18).

Interruption is mediated by a concerted action of NCX, PMCA, K,Ca and Ca,T in response to the increasing calcium concentration. But on top of changed conductivity the reversal potential plays an important role. For calcium it changes from  $22mV$  at the beginning of a burst to  $0mV$  at the end of a burst. This reduces the calcium currents through voltage-gated channels

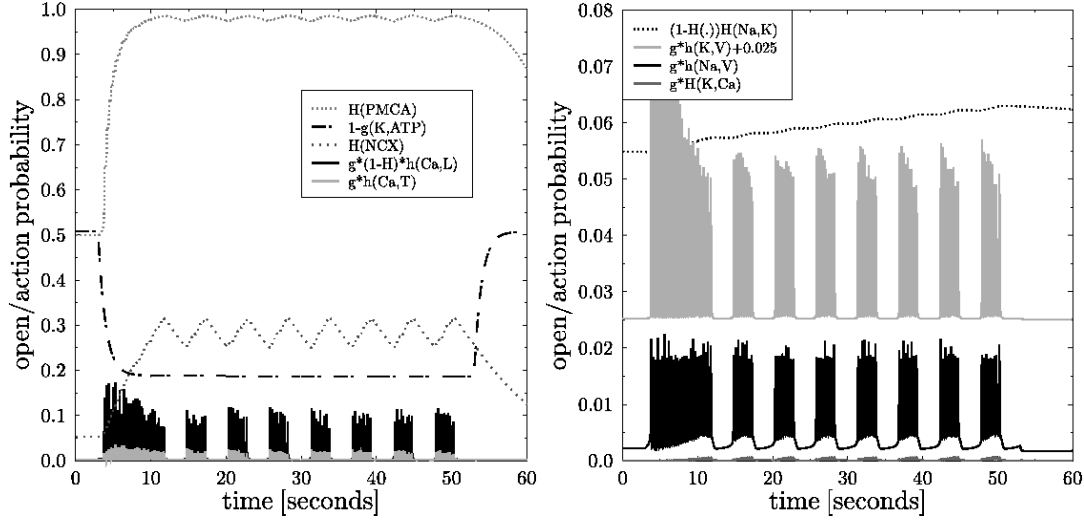


Figure 4: **Opening/activity states of the membrane proteins:** The states of the transmembrane proteins during repeated bursting as given in Figure 3 are shown as probability of activity or opening. The left panel collects all calcium-relevant proteins and the K,ATP-channel. The right panel all sodium-relevant and other potassium-conducting proteins (note the different scale in the right panel and the shifted open probability for K,V-channels). The inset lists the probabilities in the sequence of vertical appearance and gives a hint how the probabilities are calculated (see supplement Section 5.1 for details). The simulation protocol underlying this simulation is explained in the figure legend of Figure 3. Note that the PMCA-activity is at its limit in an actively bursting  $\beta$ -cell.

by about 35% (at  $V = -40mV$ ) and is a relevant contribution to the interruption of bursts. Indeed, replacing the Nernst-equation by constant reversal potentials (the ones corresponding to the resting state) leads to uninterrupted bursting (data not shown).

### 3.3 Knock-out of K,Ca-protein

The calcium-gated potassium channel K,Ca is for the first time implemented according to single membrane protein characteristics (20), which differ strongly from the values used in other models. Currently, no model for the K,Ca-opening dynamics exists. The measured opening dynamics depends on the membrane potential and the calcium concentration in a complicated way. A detailed analysis of the measured data (see supplement Section 5.1.7) has revealed that, in addition, the asymptotic opening probability for a given calcium concentration also depends on the membrane potential (see Eq. 21).

The novel model for K,Ca-opening probability is used for the  $\beta$ -cell-electrophysiology and it is predicted that under normal conditions the K,Ca-currents remain rather small because of a low opening probability. This finding suggests that K,Ca might even be unnecessary for repeated bursting. K,Ca is believed to abort burst-events when calcium is sufficiently increased.

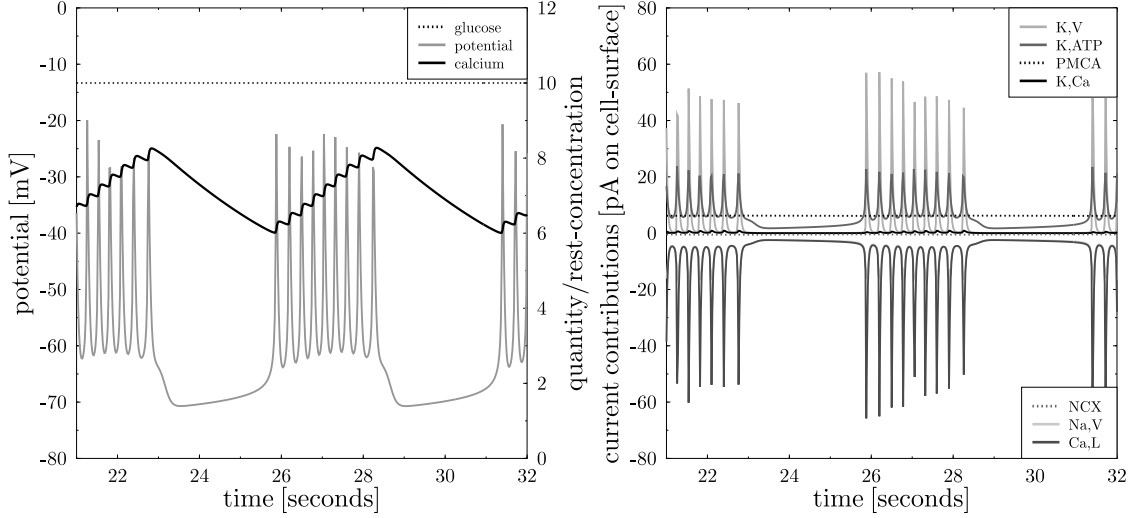


Figure 5: **High-resolution view on a burst event:** The third bursting event in Figure 3 is shown in higher resolution. All shown curves have the same meaning as explained in the legend of Figure 3.

In principle, this can also be achieved by PMCA which also directly depends on the calcium level.  $K,Ca$  is switched off ( $\rho_{K,Ca} = 0$ ) and other densities have to be slightly adapted to  $\rho_{K,ATP} = 0.13/\mu m^2$  and  $\rho_{PMCA} = 1420/\mu m^2$  in order to keep regular bursting (see Figure 6). Note that this simulation does not correspond to a block of  $K,Ca$ . The  $\beta$ -cell is constructed without  $K,Ca$ , thus, this simulation corresponds to a knock-out experiment.

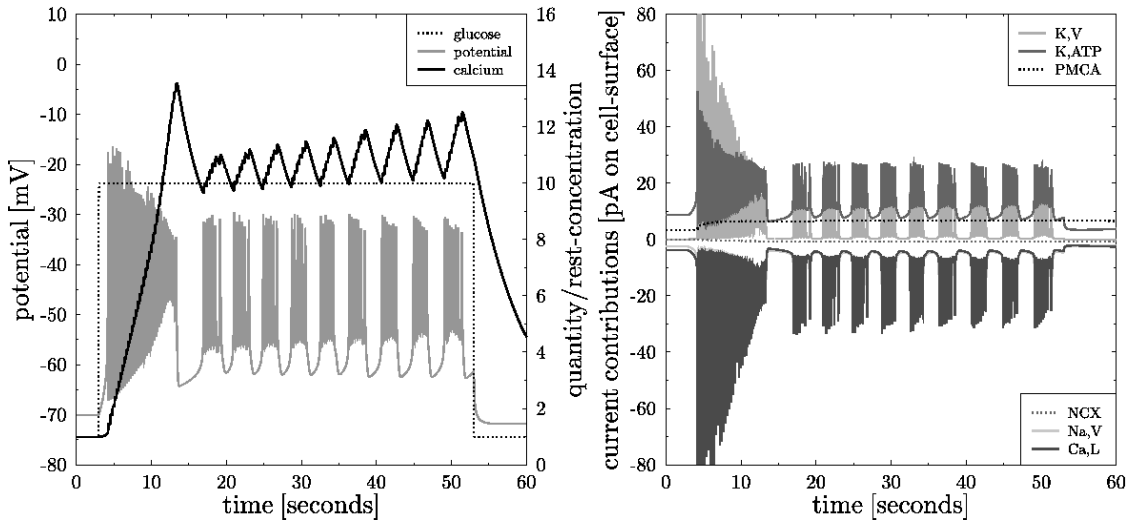


Figure 6:  **$\beta$ -cell-bursting without  $K,Ca$ -channels:** Simulation without  $K,Ca$ -channels and with protein densities adapted to  $\rho_{K,ATP} = 0.13/\mu m^2$  and  $\rho_{PMCA} = 1420/\mu m^2$ . Bursting frequency and the reached calcium level are both higher compared to Figure 3. Lines are explained in the legend of Figure 3.

In the normal  $\beta$ -cell a late increase in K,Ca-activity happens for high calcium levels (at the end of each burst, see Figure 3 and Figure 4) leading to potassium efflux. This counterbalances the calcium influx and drops depolarisation. In the present simulation without K,Ca, PMCA takes over this function. However, PMCA-activity is already at its limits during burst (see Figure 4). This is also found in the K,Ca-knock-out experiment (not shown).

The K,Ca-knock-out experiment suggests that for low calcium concentrations PMCA is the main interrupter of bursts. The interpretation that K,Ca is important for burst interruption is only supported for calcium concentration above  $500\mu M$ . In this regime PMCA is not sufficiently flexible to further increase its activity and, thus, to interrupt bursting. K,Ca is much more flexible in this respect. It will be seen later that at high calcium concentration K,Ca acquires other functionality.

### 3.4 Stimulation by raising external potassium

The effect of increased external potassium levels on  $\beta$ -cells is investigated. Starting from a  $\beta$ -cell in its resting state at normal external potassium  $K_{\text{ext}} = 5.7mM$ , external potassium is increased to different values using a steep sigmoidal function. The  $\beta$ -cell which had adapted to the lower potassium level is stimulated because the reduced chemical gradient pushes potassium into the cell and depolarises it.

For moderately increased external potassium the cell first exhibits a smooth depolarising calcium current. Larger  $K_{\text{ext}}$  then leads to K,ATP-induced action potential-like events involving potassium and calcium currents, and finally into a burst-like activity at  $K_{\text{ext}} = 8mM$ . However, this remains a unique event (data not shown). The burst is interrupted by K,Ca-activity at a rather high and constant calcium level around  $1\mu M$ . Despite a new depolarised equilibrium state which normally would induce action potentials, repeated bursting is prohibited by the constant strong activity of PMCA and K,Ca.

### 3.5 Stepwise increase of glucose levels

The full model is used to investigate the  $\beta$ -cell behaviour after stimulation with increased glucose levels. This inhibits K,ATP-potassium currents and depolarises the cell. Depending on the target glucose concentration between the resting value  $\gamma_0 = 1mM$  and  $30mM$  this becomes the germ of bursting events. The  $\beta$ -cell reaction is shown in Figure 7 for some examples. Up to  $5mM$  glucose only a smooth increase of the membrane potential is found which then stabilises on a higher level. A single action potential appears at a threshold of  $6mM$  which is in agreement with experiment (18). The spikes then turn into regular firing with increasing frequency between  $7$  and  $9mM$ . The high-frequency spikes then are interrupted and replaced by repeated bursting around  $10mM$ . The frequency of repeated bursting, the burst to silent ratio, the bursting amplitude, and the bursting baseline at  $\gamma = 10mM$  are within the range of experimental results (7, 18). For even larger glucose levels uninterrupted bursting is found which is also in agreement with experiment (7).

As in islets (18) calcium levels constantly increase with increasing glucose levels (see Figure

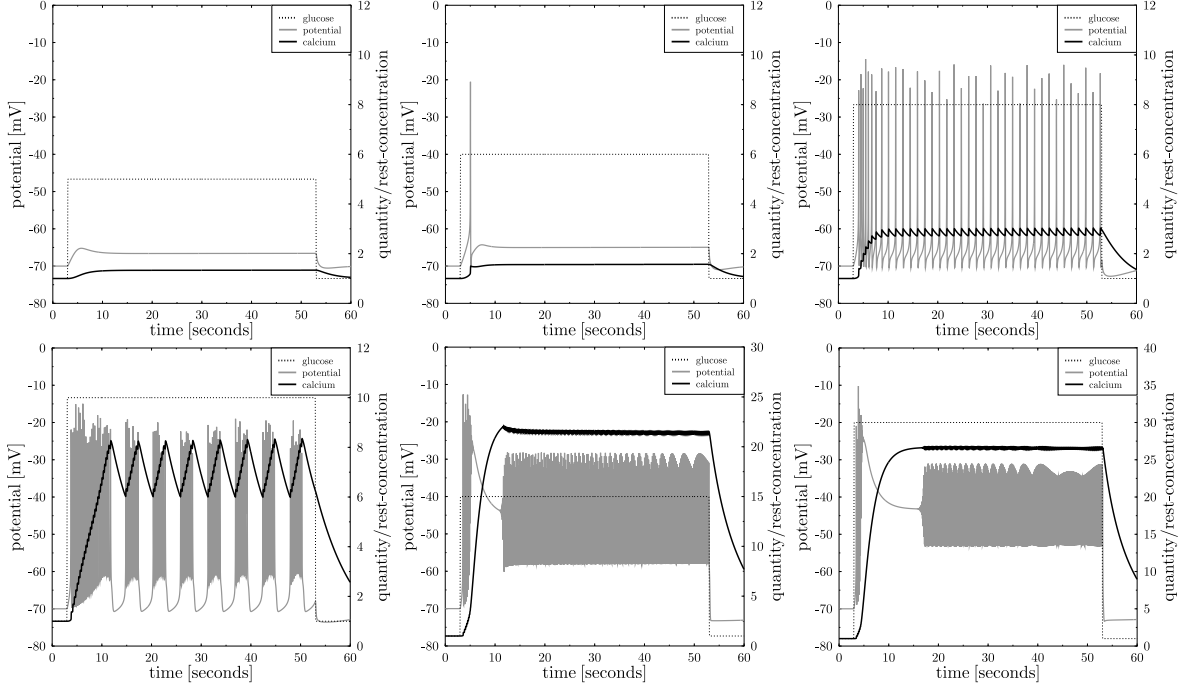


Figure 7: **The  $\beta$ -cell reaction to increased glucose levels:** Glucose stimulation is increased in several steps  $\gamma_{\text{stimulation}} = 5, 6, 8, 10, 15, 30mM$  (panels in reading order). The membrane potential (grey line) and the calcium concentration (black line) are shown. Repeated bursting is found for stimulation with about  $10mM$  glucose. Less glucose only induces single spikes, more leads to uninterrupted bursting.

7). This is not the case if the simpler model for K,Ca-activation is used (data not shown), which underlines the necessity of using the improved novel model for K,Ca-dynamics.

### 3.5.1 Steepness of glucose increases

In experiments it is observed that the initial spike or burst is more intense than the subsequently following ones – if any. According to the simulations this is related to the steepness of the switch to the higher glucose level. With smooth sigmoidal functions the initial spike can be fully suppressed. Similarly, long initial bursts can turn to a normal duration. However, the steepness of the glucose increase changes only the initial action potentials or pre-bursting events. The long-term bursting behaviour does exclusively depend on the asymptotic glucose level irrespective of how quick it is reached.

### 3.5.2 The role of K,Ca-currents at supra-large glucose

There is an unexpected diversity of model behaviour at high glucose levels in dependence of the model assumptions. Uninterrupted bursting for supra-large glucose levels is only found with the novel model for K,Ca-activation (see supplement Section 5.1.7). The simpler model for K,Ca-

activation as used in Figure 2 leads to suppression of any spike for large glucose, which is in contradiction to experiment. This underlines the necessity to rely on the measured electrophysiology of single K,Ca-channels. A rather weak role of K,Ca-channels during normal electrical activity is inferred. K,Ca gets relevantly active only at very high calcium concentrations which are associated with high glucose concentrations.

A more detailed analysis of Figure 7 reveals that uninterrupted bursting at supra-large glucose-levels is based on oscillations in the K,Ca-current. While at  $\gamma = 12mM$  the K,V-current is dominant, at  $30mM$  it is the K,Ca-channel which provides the largest contribution to the potassium current (see Figure 8). Instead of K,V and Ca,L it is now K,Ca and Ca,L which are

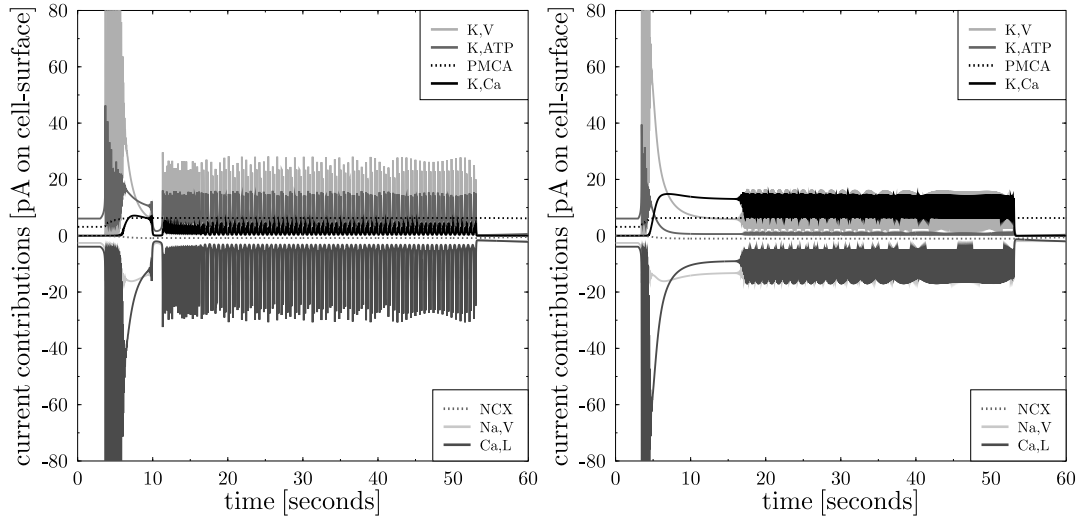


**Figure 8: K,Ca is the main oscillator at large glucose levels:** The current contributions of K,Ca and K,V to uninterrupted bursting for glucose levels of 12 (left) and  $30mM$  (right) are shown. While at  $12mM$  the main contributors to the oscillations are K,V (light grey full line) and Ca,L (grey full line), these are K,Ca (black full line) and Ca,L at  $30mM$  glucose. Note also that the contribution of K,ATP-channels is strongly reduced at supra-high glucose levels.

swinging. This result suggests an additional role of K,Ca-channel in the electrophysiology of the  $\beta$ -cell: It defines the electrical activity at supra-large glucose and calcium concentrations.

### 3.6 Inhibit SERCA-activity

Thapsigargin is a SERCA-inhibitor. Its effect is to elevate the intracellular baseline calcium concentration. It was found that thapsigargin can induce continuous firing in  $\beta$ -cells (7). As the present simulation does not include the ER explicitly SERCA-block is mimicked by induction of its effect on the calcium baseline. To this end the calcium leakage current in a cell with established resting state is modified.

A reduction of the leakage current to 20%, indeed, leads to an increased baseline calcium level. If then glucose is turned to  $\gamma = 10mM$  continuous bursting is found. When the leakage current



is turned back to its resting state value normal repeated bursting is recovered (see Figure 9). Continuous bursting is also found if the leakage current is reduced after repeated bursting being

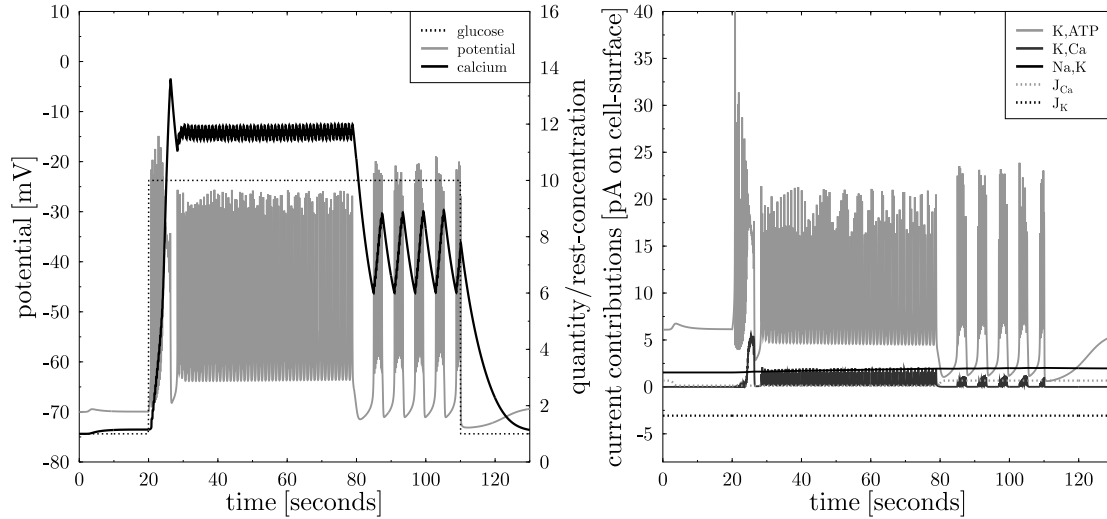


Figure 9: **Reduction of leakage current to mimic SERCA-block:** The calcium leakage current is reduced to 20% at 3s to mimic SERCA-blocking (right panel, grey dotted line). This increases the calcium baseline (left panel, black line). At  $t = 20s$  glucose is turned to  $\gamma = 10mM$  (left panel, black dotted line), which induces continuous bursting (left panel, grey line). At  $t = 80s$  the leakage current is turned back to normal and repeated bursting (as in Figure 3) is recovered. At  $t = 110s$  glucose is turned back to its resting value. The right panel shows all but K,V whole cell potassium currents. Note that because of its stoichiometry Na,K-potassium current has negative sign and double absolute value with respect to the shown curve (right panel, black full line).

already established at high glucose levels. Thus, the sequence of stimulation events is not important.

From Figure 9 it can be read off that the K,Ca-current is increased during continuous bursting as compared to repeated bursting. In contrast, the K,ATP-current is smaller during continuous bursting. This is in agreement with the results found in (7), Figure 4 therein. However, the interpretation is different: The authors in (7) suspected that the reduced consumption of ATP (during SERCA block) leads to less inhibition of K,ATP-channels. The simulation suggests that the increased calcium baseline increases the necessary PMCA pumping activity in order to establish a steady-state. In fact, the consumed amount of ATP is more related to the absolute calcium level in the cell than to the number of blocked ATPases. Thus, the present simulation suggests that altered calcium concentrations and membrane potentials during block of SERCA reduce K,ATP-currents independent of the intracellular ATP-concentration.

### 3.7 Partial blocking of PMCA and NCX

A very similar result (to Figure 9) is found when the PMCA-current is reduced to 90%. The calcium baseline is increased and at  $10mM$  glucose uninterrupted bursting is found. Substantially stronger inhibition of PMCA-activity suppresses bursting after an initial bursting event (data not shown).

A reduction of the NCX-current to 80% also leads to uninterrupted bursting. However, the characteristics are different. As before the calcium baseline is increased. But, instead of an increased calcium level during uninterrupted bursting, the calcium level is decreased (data not shown). This points to two different mechanisms both leading to uninterrupted bursting.

### 3.8 Block $K_{ATP}$ with tolbutamide

Block of  $K_{ATP}$ -currents was investigated in patch-clamp experiments with  $\beta$ -cells in intact islets (7). *In silico* the application of tolbutamide corresponds to a reduction of the  $K_{ATP}$  protein density  $\rho_{K,ATP}$  in a cell that has established its steady state in the presence of normal  $K_{ATP}$ -presence. A reduction of  $K_{ATP}$ -currents to 75% leads to a result almost identical to Figure 9. An increased calcium baseline is established. This happens because the reduced potassium outflow depolarises the cell which, in turn, partially opens voltage-dependent calcium channels. The new equilibrium state is, thus, established on a higher level of calcium influx.

When glucose is increased to  $10mM$  uninterrupted bursting is induced. As in experiment (7) this is reversible: After release of partial  $K_{ATP}$ -block normal repeated bursting behaviour is reestablished. This happens in the simulation without any additional stimulation. In (7) the  $\beta$ -cell was depolarised several times in voltage clamp mode.

Note that an overexpression of  $K_{ATP}$ -channels also leads to uninterrupted bursting despite the fact that the calcium baseline is decreased (data not shown). Again this points to at least two mechanisms for uninterrupted bursting. For even more increased  $K_{ATP}$ -currents regular single firing is observed.

Interestingly, a total block of  $K_{ATP}$ -channels immediately leads to continuous bursting even at the resting glucose concentration  $\gamma_0 = 1mM$  (see Figure 10). This supports that these channels trigger bursting events by inhibition of potassium outwards currents. The observed independence of the increased glucose level at  $t = 20s$  is a direct consequence of the fact that in the model  $K_{ATP}$ -channels are the only point of effect of glucose. ATP-ADP ratios are not explicitly monitored which would also change ATPase activities.

It is possible to stimulate  $\beta$ -cells by partial block of  $K_{ATP}$ -currents. Repeated bursting is induced at resting glucose level (see Figure 10, right panel, for a 50%-block). When glucose is increased at  $t = 20s$  repeated bursting turns into uninterrupted bursting.

### 3.9 Modulation of voltage-gated calcium channels

While overexpression of LVA calcium channels  $Ca_T$  leads to similar results as shown in Figure 9, block or knock-out of LVA channels has only minor effect on the bursting behaviour.

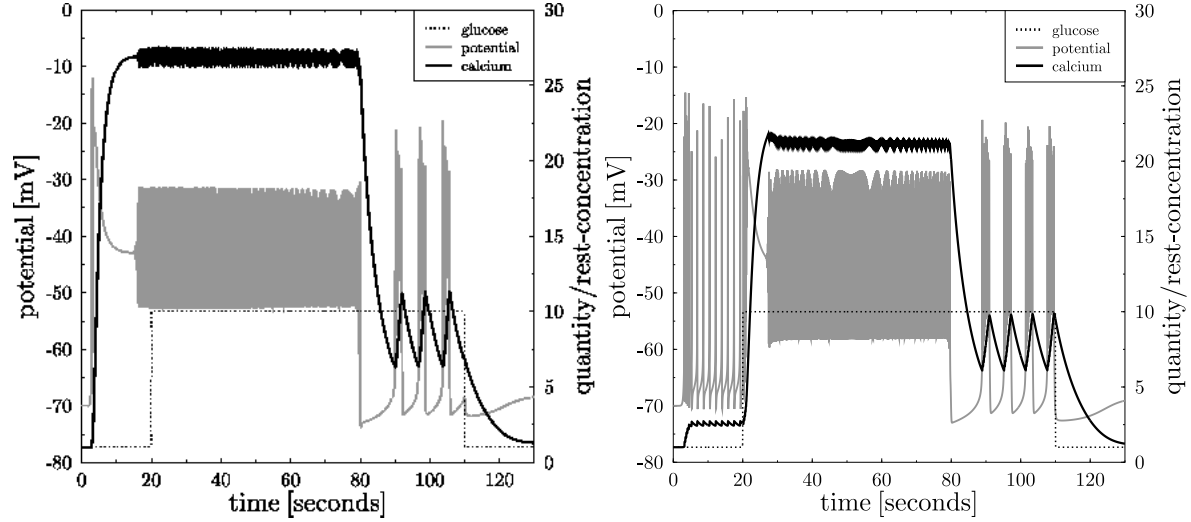


Figure 10: **Total and partial block of K,ATP:** K,ATP is fully blocked at  $t = 3s$  (left panel). This induces strong depolarisation, calcium inflow and continuous bursting. At  $t = 20s$  glucose is turned to  $\gamma = 10mM$ , which does not influence bursting for lack of K,ATP. At  $t = 80s$  the block of K,ATP is released and repeated bursting is recovered (as found in Figure 3). At  $t = 110s$  glucose is turned back to its resting value. The right panel shows the result of partial block of K,ATP-channels to 50% using the otherwise same protocol. High frequency repeated bursting is found at resting glucose levels.

Inhibition only weakly modifies the calcium baseline before stimulation with glucose. The amplitude of spikes of the membrane potential is slightly increased and the reached calcium level is slightly shifted (data not shown). Thus, according to the present simulations, LVA have to be considered unimportant for  $\beta$ -cell-bursting.

However, this is a weak statement because for a different set of densities (with a larger fraction of LVA channels) the role of LVA calcium channels is more pronounced. In particular, the inactivation of Ca,T (note that HVA Ca,L-type calcium channels inactivate only slowly) might play a role for interruption of bursting events. In these simulations uninterrupted bursting is found for weak and for total inhibition of LVA-currents. The present simulation does not yet allow to make precise statements on the importance of LVA channels and on their inactivation. However, it can be stated that if Ca,T-type channels were expressed to a relevant amount in  $\beta$ -cell, their inactivation properties would have impact on the interruption of bursting events. This is further supported by the observation that 70% of the calcium current in whole- $\beta$ -cell-experiments is inactivated after  $100ms$  (19), which is impossible on the basis of Ca,L-channels that show only little or no inactivation. It would be most interesting to get data about the ratio of LVA and HVA calcium channels in  $\beta$ -cells.

Moderate inhibited or strengthened Ca,L-currents also lead to uninterrupted bursting combined with an increased or lowered calcium baseline, respectively (data not shown). For stronger inhibition (20% remaining) spiking activity disappears, which is consistent with the dominant role of the Ca,L-current for  $\beta$ -cell-oscillations.

### 3.10 Modulation of sodium currents

The sodium-potassium exchanger Na,K uses ATP to transport both sodium and potassium against their electrochemical gradient. Even though this membrane protein is only weakly active in the resting state, shows little dynamics upon  $\beta$ -cell stimulation (variation of intracellular potassium concentration is relatively small), and induces only small currents, the bursting behaviour is sensitive to partial blocking of the exchanger. Already at 70% of the Na,K-current uninterrupted bursting is found. This comes with a comparably small increase in the calcium baseline. Uninterrupted bursting is also found for increased Na,K-currents (130% or more). Interestingly, the calcium baseline is decreased in this scenario, and, thus, cannot be at the origin of uninterrupted bursting. Note that due to the weak dynamics of Na,K-currents corresponding effects are not found in Na,K-knock-out experiments.

Similarly the voltage-dependent sodium channel Na,V is generally not considered to play a major role in  $\beta$ -cell electrophysiology. At a partial block to 80% (or lower) uninterrupted bursting is found together with a slightly reduced calcium baseline (see Figure 11 left panel). Uninterrupted bursting is also found if the Na,V-currents are increased by a factor 1.3 or higher together with a slightly increased calcium baseline (see Figure 11 right panel).

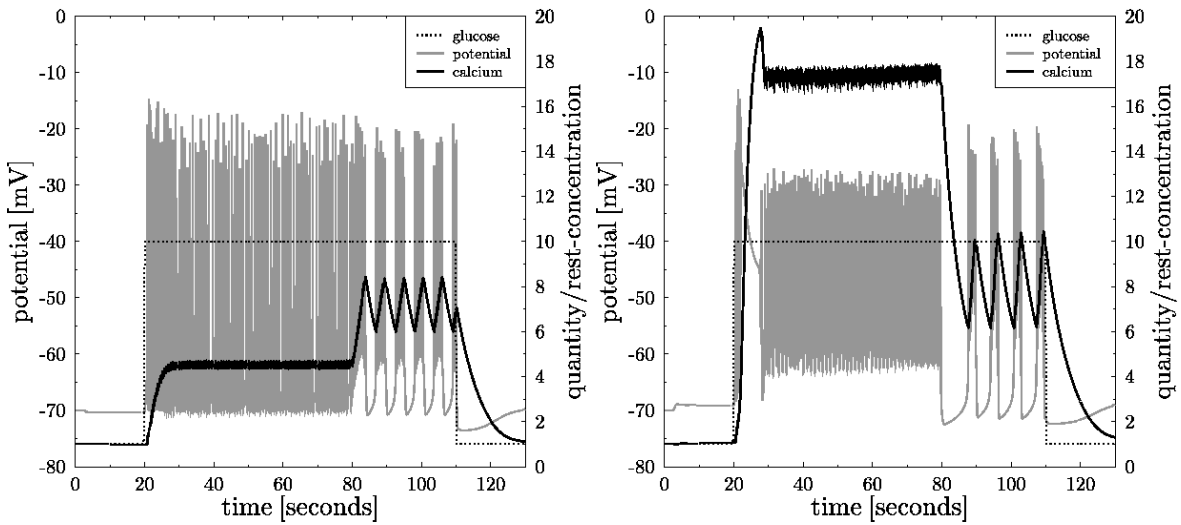


Figure 11: **Modulating Na,V-currents:** Na,V-currents are inhibited to 90% (left panel) and increased to 130% (right panel) using the same protocol as in Figures 9 and 10. The calcium baseline (full black line) is reduced and increased, respectively. At  $10mM$  glucose (see  $t > 20s$ ) uninterrupted bursting is found in both cases with differing characteristics. While uninterrupted bursting with increased calcium baseline is similar to Figure 9, amplitude and burst baseline are different when coming together with a reduced calcium baseline. This points to different mechanisms leading to uninterrupted bursting.

Why is uninterrupted bursting found with reduced calcium baseline when either Na,K-currents are increased or Na,V-currents are reduced? Both, increased Na,K- and reduced Na,V-currents polarise the cell because intracellular sodium levels are reduced. This reduces the calcium

influx through voltage-gated calcium channels, and, in turn, reduces the calcium baseline. In the same way intracellular potassium levels are increased because of less potassium efflux. This corresponds to a pre-stimulation in complete analogy to the inhibition by K,ATP-channels.

Thus, we have to distinguish low and high calcium uninterrupted bursting.  $\beta$ -cells become prone to oscillations either by increased calcium baseline or by increased potassium baseline. The equilibrium of both is regulated by the sodium-currents. Despite the sodium conducting proteins playing an unspectacular role in  $\beta$ -cell activity they nevertheless influence the electrophysiology in an unexpected strength.

### 3.11 Modulation of potassium currents

Inhibition of K,Ca-currents reduces the burst to silence ratio and the bursting frequency. Even at currents of 10% repeated bursting is still observed. Only when K,Ca-currents are totally blocked, bursting is fully suppressed. Increased K,Ca-currents lead to increased burst to silence ratios and at 150% to uninterrupted bursting (the characteristics correspond to those as found in Figure 11 left panel). The calcium baseline and the membrane potential are not visibly altered by modulation of the K,Ca-currents (data not shown).

Increased K,V-currents lead to uninterrupted bursting. A reduction of K,V-currents reduces the burst to silence ratio. Surprisingly, even with totally blocked K,V-currents, oscillations are still found with almost unaltered calcium baseline. The potassium current in the action potentials is then taken over by the K,Ca-currents. This shows that K,Ca-proteins have the potential to drive the oscillations during burst events – similar to the scenario found for supra-large glucose levels.

### 3.12 Long-term stimulation

Stimulation by increased glucose levels not only induce repeated bursting, the  $\beta$ -cell is also shifted out of its resting state. If stimulation by glucose is applied for long durations, and assuming in a thought experiment all other cell properties unaltered during that period, the  $\beta$ -cell might find a novel stable resting state which is in equilibrium with the high glucose level. The simulation in Figure 3 is repeated with 10mM glucose applied for one hour. Due to limited responsiveness of Na,K-exchangers each burst event (involving Na,V-current oscillations) increases the intracellular sodium level. After half an hour sodium reaches a novel resting state at 170% of its resting concentration adopted to the ongoing stimulation (data not shown). Similarly the intracellular potassium concentration decreases to a new equilibrium state. Now, Na,K-activity and sodium inflow at each bursting event get into equilibrium. Repeated bursting is still present at this higher sodium-state. Only the baseline of bursts is increased by about 20mV.

## 4 Discussion

### *A bottom-up approach for the $\beta$ -cell with quantitative ambitions*

A simulation tool for the electrophysiology of  $\beta$ -cell was introduced. The model is strictly based on experimental data for single membrane protein activity or conductivity measurements. This is considered to be a first step towards a quantitative modelling of  $\beta$ -cell electrical activity. Previous modelling work either structurally considered only those elements necessary to induce repeated bursting or omitted some essential protein properties. All previous models relied on whole-cell experiments. Thus, the present model can be considered to be the first bottom-up approach of the  $\beta$ -cell starting at the molecular level and predicting emerging properties on the cellular scale.

### *Improvements with respect to other modelling approaches*

The present model, besides on relying on single protein characteristics, includes several  $\beta$ -cell-properties that have been neglected in previous modelling approaches. It was found that the back-reaction of the PMCA-currents on the membrane potential are very important and strongly alter bursting behaviour as found in (1, 3). The inactivation properties (neglected in (2)) of the channels turn out to be relevant for burst interruption and the stability of oscillation. Finally, the Nernst-equation was used to dynamically calculate the reversal potential (which was assumed constant in (1, 3, 5)) and turned out to substantially change the currents during burst events.

### *The endoplasmatic reticulum might change the dynamics*

Even though a block of processes related to the endoplasmatic reticulum does not affect  $\beta$ -cell oscillations (17), calcium-induced-calcium-release might well modify the dynamics of raising calcium. These modifications might lead to adaptations of protein densities. Also the simple minded cell geometry has impact on the protein densities. Thus, even though the resulting whole-cell currents are realistic, the protein densities used in the simulations (see Tab. 5 in the supplement) are not considered as a quantitative prediction in the present stage of the model. Note that calcium pumps in the endoplasmatic reticulum will in first approximation act as an additional sink of free calcium which, in the present model, is effectively included in a large concentration of calcium binding sites.

### *Characteristics of glucose-dependent $\beta$ -cell-stimulation are reproduced*

Despite the necessity for further improvement, the agreement with current experimental data is rather convincing and strengthens the relevance of the found results. The calcium response is of similar strength, and whole cell currents are in the right range (19). Bursting is found in the same regime of glucose levels as in experiment (7, 18). The glucose threshold for  $\beta$ -cell electrical response is quantitatively reproduced to be around  $5mM$  (18). The bursting frequency is in the range of experimental data. Uninterrupted bursting is found for large glucose levels as in experiment (7). Thus, it can be stated that the simulation respects the relevant characteristics of repeated bursting in  $\beta$ -cells.

### *The range of glucose leading to bursting is too small*

A more detailed analysis reveals quantitative deviations between simulation and experiment. The most relevant one concerns the range of glucose for which repeated bursting is found. While the simulation predicts 9 to  $11mM$  in experiment the lower limit is at  $7mM$  (18) and the upper limit at  $15mM$  (7). This discrepancy might be explained by a structural difference



between the experimental set-up and the simulation: The simulation models single  $\beta$ -cells, while both cited experiments investigate  $\beta$ -cell in a context of intact islets. Repeated bursting is difficult to be induced in isolated  $\beta$ -cells, which can explain why the range of glucose is so small in the simulations. It has to be evaluated in future research whether the gap-junction-mediated contact to other  $\beta$ -cells can enlarge the glucose regime for repeated bursting.

#### *A novel model of $\beta$ -cell-bursting*

The fact that the main properties of  $\beta$ -cell-electrophysiology are correctly described by the simulation encourages to draw a novel picture of how  $\beta$ -cell-bursting emerges. This picture is presented as a sequence of events:

- **Glucose inhibits K,ATP:** Increased glucose only gives a short pulse of inhibition of K,ATP-currents. This slightly depolarises the  $\beta$ -cell which is further amplified by induced sodium and calcium entry through voltage-gated channels (Na,V; Ca,L; and Ca,T).
- **K,ATP-currents increase again:** Even though the opening of K,ATP-channels is inhibited the current increases upon cell depolarisation. According to Eq. 14 (see supplement) inhibition is over-compensated by the increased electrochemical gradient.
- **Ca,L and Na,V cause electrical spiking:** If the stimulus is over-critical a spike of cell depolarisation is induced by voltage-dependent calcium and sodium currents.
- **Oscillations are induced by delayed K,V-response:** The potassium current repolarises the cell, but this happens only with a delay  $\tau_{K,V}$ . It is well known that delayed response can lead to stable fast oscillations.
- **Calcium rises during the burst:** During a bursting event calcium and sodium is constantly entering the cell while potassium is leaving it. While the effect on potassium and sodium is small, calcium rises because of a strong electrochemical gradient and the small resting concentration. The speed of calcium increase is controlled by the intracellular calcium buffer, and is much slower than the oscillations.
- **The burst is interrupted by a concerted action of Nernst-reversal potential, PMCA, NCX, K,Ca and Ca,T:** During bursts calcium levels increase and the calcium reversal potential is reduced. The latter inhibits the calcium-currents, while the first increase repolarising PMCA-, NCX-, and K,Ca-currents, where K,Ca-currents play a minor role at normal calcium levels (20). At a critical calcium concentration and reversal potential oscillations are suppressed. The interruption of bursts is facilitated by the inactivation dynamics of LVA calcium channels.
- **Uninterrupted bursting is driven by K,Ca:** As also K,Ca acts with a certain delay this membrane protein has totally analogous potential to drive oscillations with Na,V- and Ca,L-mediated depolarising currents. According to the measured activity characteristics (20) oscillations are possible at large calcium concentrations only and can even drive uninterrupted bursting.
- **Repolarisation after burst events is governed by PMCA, NCX, and Na,K:** In complete analogy to neuronal repolarisation, ATPases and exchangers are needed to reestab-



lish the resting concentrations. However, sodium and potassium are continuously changing their level during long stimulation.

Note that this model differs from older models in several aspects which are discussed in more detail in the following.

*Sodium currents are important regulators of  $\beta$ -cell-electrophysiology*

Na,V-currents directly participate in spikes and bursting events. The activity of the  $\beta$ -cell is responsive to all properties of the Na,V-channel. Thereby the half activation potential  $V_{Na,V}$  has the greatest influence. Na,V-currents facilitate onset of action potentials due to their fast dynamics (the reaction time is the fastest of all considered channels), participate in the interplay with delayed potassium currents to induce oscillations, and also facilitates the end of action potentials by relatively fast inactivation. The interpretation of a tightly controlled interplay of Na,V with other membrane proteins is supported by the observation that uninterrupted bursting is observed for partially blocked *and* overexpressed Na,V-proteins. The latter bursting is characterised by high calcium, the former by high potassium. It turns out that Na,V-currents regulate the equilibrium between both ions in  $\beta$ -cell-stimulation. According to the model results sodium channels are more relevant for the  $\beta$ -cell electrophysiology than previously expected.

*Long-term stimulation gives rise to a third time scale*

The *in silico* experiment of long term stimulation of  $\beta$ -cells with high levels of glucose has revealed three time scales of  $\beta$ -cell-electrophysiology:

1. Delay of K,V or K,Ca currents with respect to calcium and sodium induced depolarisations (10 – 100ms),
2. slow increase in intracellular calcium level due to intense buffering which keeps the fraction of free calcium low (10s), and
3. even slower modifications of intracellular sodium and potassium levels (10min).

The third time scale should be observable in experiment.

*Glucose only induces a tiny inhibition of K,ATP-currents*

In the model the only effect of increased glucose levels is inhibition of K,ATP-currents. However, the inhibition turns out to be a tiny effect which quickly is hidden by the increased K,ATP-currents in response to cell depolarisation. This opens the possibility of alternative effects of glucose via ATP-metabolism. Several channels and transporters rely on ATP-concentrations and may alter their activity in response to changed glucose levels. Some might well initiate bursting as already established for K,ATP. This might explain the recently observed insulin secretion and calcium dynamics in islets of mice lacking K,ATP-activity (21).

*Bursts are interrupted by NCX, PMCA, Ca,T and the dynamic reversal potential*

Interruption of bursting only weakly rely on K,Ca-currents because of small activity at physiological calcium levels. Instead, interruption is strongly related to NCX and PMCA activity. Mostly neglected in former research is the impact of a dynamic calcium reversal potential (see Eq. 5) which turns out to change the calcium currents by about 35% during a burst. The inactivation dynamics of LVA calcium channels Ca,T also supports burst interruption. The latter

statement depends on the ratio of LVA- and HVA-channels in  $\beta$ -cell, which would be important to be measured. In summary, burst interruption seems not to rely on a single type of membrane proteins but on a concerted action of various factors.

#### *Calcium driven potassium channels K,Ca can drive oscillations*

For the first time it is postulated that K,Ca is an active part of the bursting behaviour as well. Thereby the unknown K,Ca-time scale of activation is relevant: If the K,Ca adapts faster to the membrane potential (thus using a smaller  $\tau_{K,Ca}$ ) the currents get out of phase and uninterrupted bursting is destroyed. Therefore, the measurement of  $\tau_{K,Ca}$  is most important to learn about this predicted functionality of K,Ca-currents. According to the simulation results K,Ca acquire a major role for very large calcium concentrations where it takes over the role of K,V in oscillations.

#### *Falsification of the predictions of the simulation*

On one hand an improved version of the simulation model has to be developed in order to see whether the predictions of the simulations and the attributed roles of various membrane proteins for  $\beta$ -cell electrical activity are robust. The improved model shall include the impact of intracellular calcium stores and explicitly model the dynamics of ATP. On the other hand some of the *in silico* experiments were not executed in real systems. The simulation tool might serve as a guide for the design of very focused and conclusive experiments. This is not restricted to the proposed experiments. On the contrary the author welcomes the challenge of the simulation model with further suggestions for experimental set-ups.

**Acknowledgments:** Michael Meyer-Hermann thanks Michele Solimena for pointing me to the subject. MMH is indebted to Michele Solimena and Marc Thilo Figge for regular and fruitful discussion and for revising the manuscript. FIAS is supported by the ALTANA AG. MMH is supported by the EC-NEST-project MAMOCCELL.

## References

1. Chay, T., and J. Keizer. 1983. Minimal model for membrane oscillations in the pancreatic  $\beta$ -cell. *Biophys. J.* 42:181–190.
2. Fridlyand, L., N. Tamarina, and L. Philipson. 2003. Modeling of  $Ca^{2+}$  flux in pancreatic beta-cells: role of the plasma membrane and intracellular stores. *Am. J. Physiol. Endocrinol. Metab.* 285:E138–E154.
3. Sherman, A., J. Rinzel, and J. Keizer. 1988. Emergence of organized bursting in clusters of pancreatic beta-cells by channel sharing. *Biophys. J.* 54:411–425.
4. Chay, T. R. 1997. Effects of extracellular calcium on electrical bursting and intracellular and luminal calcium oscillations in insulin secreting pancreatic  $\beta$ -cells. *Biophys. J.* 73:1673–1688.
5. Bertram, R., and A. Sherman. 2004. A calcium-based phantom bursting model for pancreatic islets. *Bull. Math. Biol.* 66:1313–1344.

6. Keizer, J., and G. Magnus. 1989. ATP-sensitive potassium channel and bursting in the pancreatic beta cell. A theoretical study. *Biophys. J.* 56:229–242.
7. Kanno, T., P. Rorsman, and S. Gopel. 2002. Glucose-dependent regulation of rhythmic action potential firing in pancreatic beta-cells by K(ATP)-channel modulation. *J. Physiol.* 545.2:501–507.
8. Ashcroft, F., D. Harrison, and S. Ashcroft. 1984. Glucose induces closure of single potassium channels in isolated rat pancreatic  $\beta$ -cells. *Nature.* 312:446–448.
9. Cook, D., and C. Hales. 1984. Intracellular ATP directly blocks K<sup>+</sup> channels in pancreatic B-cells. *Nature.* 311:271–273.
10. Erler, F., M. Meyer-Hermann, and G. Soff. 2004. A quantitative model for presynaptic free calcium dynamics during different stimulation protocols. *Neurocomputing.* 61:169–191.
11. Hille, B. 1992. *Ionic Channels of Excitable Membranes*, 2nd Ed. Sinauer Ass. Inc.
12. Fridlyand, L., L. Ma, and L. Philipson. 2005. Adenine nucleotide regulation in pancreatic beta-cells: modeling of ATP/ADP-Ca<sup>2+</sup> interaction. *Am. J. Physiol. Endocrinol. Metab.* 289:E839–E848.
13. Hopkins, W., S. Fatherazi, B. Peter-Riesch, B. Corkey, and D. Cook. 1992. Two sites for adenine-nucleotide regulation of ATP-sensitive potassium channels in mouse pancreatic beta-cells and HIT cells. *J. Membr. Biol.* 129:287–295.
14. Detimary, P., P. Gilon, and J. Henquin. 1998. Interplay between cytoplasmic Ca<sup>2+</sup> and the ATP/ADP ratio: a feedback control mechanism in mouse pancreatic islets. *Biochem. J.* 333:269–274.
15. Ämmälä, C., O. Larsson, P.-O. Berggren, K. Bokvist, L. Juntti-Berggren, H. Kindmark, and P. Rorsman. 1991. Inositol trisphosphate-dependent periodic activation of a Ca<sup>2+</sup>-activated K<sup>+</sup> conductance in glucose-stimulated pancreatic beta-cells. *Nature.* 353:849–852.
16. Liu, Y., E. Grapengiesser, E. Gylfe, and B. Hellman. 1995. Glucose induces oscillations of cytoplasmic Ca<sup>2+</sup>, r<sup>2+</sup> and Ba<sup>2+</sup> in pancreatic beta-cells without participation of the thapsigargin-sensitive store. *Cell Calcium.* 18:165–173.
17. Gilon, P., A. Arredouani, P. Gailly, J. Gromada, and J.-C. Henquin. 1999. Uptake and release of Ca<sup>2+</sup> by the endoplasmic reticulum contribute to the oscillations of the cytosolic Ca<sup>2+</sup> concentration triggered by Ca<sup>2+</sup> influx in the electrically excitable pancreatic B-cell. *J. Biol. Chem.* 274:20197–20205.
18. Beauvois, M., C. Merezak, J. Jonas, M. Ravier, J. Henquin, and P. Gilon. 2006. Glucose-induced mixed [Ca<sup>2+</sup>]<sub>i</sub> oscillations in mouse beta-cells are controlled by the membrane potential and the SERCA3 Ca<sup>2+</sup>-ATPase of the endoplasmic reticulum. *Am. J. Physiol. Cell Physiol.* 209:C1503–1511.

19. Goepel, S., T. Kanno, S. Barg, J. Galvanovskis, and P. Rorsman. 1999. Voltage-gated and resting membrane currents recorded from B-cells in intact mouse pancreatic islets. *J. Physiol.* 521:717–728.
20. Barrett, J., K. L. Magleby, and B. Pallotta. 1982. Properties of single calcium-activated potassium channels in cultured rat muscle. *J. Physiol.* 331:211–230.
21. Szollosi, A., M. Nenquin, L. Aguilar-Bryan, J. Bryan, and J. Henquin. 2007. Glucose stimulates  $\text{Ca}^{2+}$  influx and insulin secretion in 2-week-old beta-cells lacking ATP-sensitive  $\text{K}^{+}$  channels. *J. Biol. Chem.* 282:1747–1756.
22. Chapman, J., J. E., and J. Kootsey. 1983. Electrical and biochemical properties of an enzyme model of the sodium pump. *J. Membr. Biol.* 74:139–153.
23. Owada, S., O. Larsson, P. Arkhammar, A. Katz, A. Chibalin, P.-O. Berggren, and A. Bertorello. 1999. Glucose Decreases  $\text{Na}^{+}$ ,  $\text{K}^{+}$ -ATPase activity in Pancreatic beta-Cells. *J. Biol. Chem.* 274:2000–2008.
24. Maixent, J., and I. Berrebi-Betrand. 1993. Turnover rates of the canine cardiac  $\text{Na}$ ,  $\text{K}$ -ATPases. *FEBS Lett.* 330:297–301.
25. Bezanilla, F. 1987. Single sodium channels from the squid giant axon. *Biophys. J.* 52:1087–1090.
26. Plant, T. 1988.  $\text{Na}^{+}$  currents in cultured mouse pancreatic B-cells. *Pflug. Arch.* 411:429–435.
27. Hiriart, M., and D. Matteson. 1988.  $\text{Na}$  channels and two types of  $\text{Ca}$  channels in rat pancreatic B cells identified with the reverse hemolytic plaque assay. *J. Gen. Physiol.* 91:617–639.
28. Dunne, M., C. Ammala, S. Straub, and G. Sharp. 2001. Electrophysiology of the pancreatic b-cell and the mechanisms of inhibition of insulin release. *In Handbook of Physiology: The Endocrine Pancreas and Regulation of Metabolism.* A. Jefferson, L.S.; Cherrington, editor. Oxford University Press. 79–123.
29. Magee, J., and D. Johnston. 1995. Characterization of single voltage-gated  $\text{Na}^{+}$  and  $\text{Ca}^{2+}$  channels in apical dendrites of rat CA1 pyramidal neurons. *J. Physiol.* 487:67–90.
30. Juhaszova, M., P. Church, M. P. Blaustein, and E. F. Stanley. 2000. Location of calcium transporters at presynaptic terminals. *Eur. J. Neurosci.* 12:839–846.
31. Blaustein, M., and W. Lederer. 1999. Sodium/calcium exchange: its physiological implications. *Physiol. Rev.* 79:763–854.
32. del Principe, F., M. Egger, and E. Niggli. 1999. Calcium signalling in cardiac muscle: refractoriness revealed by coherent activation. *Nature Cell Biol.* 1:323–329.
33. Gall, D., and I. Susa. 1999. Effect of  $\text{Na}/\text{Ca}$  exchange on plateau fraction and  $[\text{Ca}]_i$  in models for bursting in pancreatic beta-cells. *Biophys. J.* 77:45–53.

34. DiPolo, R., and L. Beaugé. 2002. Ionic ligand interactions with the intracellular loop of the sodium-calcium exchanger. Modulation by ATP. *Prog. Biophys. Mol. Biol.* 80:43–67.
35. Váradi, A., E. Molnár, and J. Ashcroft. 1995. Characterisation of endoplasmic reticulum and plasma membrane  $\text{Ca}^{2+}$ -TPases in pancreatic beta-cells and in islets of Langerhans. *Biochim. Biophys. Acta.* 1236:119–127.
36. Caride, A., A. Filoteo, A. Penheiter, K. Paszty, A. Enyedi, and J. Penniston. 2001. Delayed activation of the plasma membrane calcium pump by a sudden increase in  $\text{Ca}^{2+}$ : fast pumps reside in fast cells. *Cell Calcium.* 30:49–57.
37. Carafoli, E. 1991. The calcium pumping ATPase of the plasma membrane. *Annu. Rev. Physiol.* 53:531–547.
38. Caride, A., A. Penheiter, A. Filoteo, Z. Bajzer, A. Enyedi, and J. Penniston. 2001. The plasma membrane calcium pump displays memory of past calcium spikes. Differences between isoforms 2b and 4b. *J. Biol. Chem.* 276:39797–39804.
39. Graupner, M., F. Erler, and M. Meyer-Hermann. 2005. A theory of Plasma Membrane Calcium Pump stimulation and activity. *J. Biol. Phys.* 31:183–206.
40. Elwess, N., A. Filoteo, A. Enyedi, and J. Penniston. 1997. Plasma membrane  $\text{Ca}^{2+}$  pump isoforms 2a and 2b are unusually responsive to calmodulin and  $\text{Ca}^{2+}$ . *J. Biol. Chem.* 272:17981–17986.
41. Rorsman, P., and E. Renstrom. 2003. Insulin granule dynamics in pancreatic beta cells. *Diabetologia.* 46:1029–1045.
42. Kelly, R., R. Sutton, and F. Ashcroft. 1991. Voltage-activated calcium and potassium currents in human pancreatic beta-cells. *J. Physiol.* 443:175–192.
43. Vinet, R., and F. F. Vargas. 1999. L- and T-type voltage-gated  $\text{Ca}^{2+}$  currents in adrenal medulla endothelial cells. *AJP - Heart and Circulatory Physiology.* 276:H1313–H1322.
44. Smith, P., F. Ashcroft, and C. Fewtrell. 1993. Permeation and gating properties of the L-type calcium channel in mouse pancreatic beta cells. *J. Gen. Physiol.* 101:767–797.
45. Plant, T. 1988. Properties and calcium-dependent inactivation of calcium currents in cultured mouse pancreatic B-cells. *J. Physiol.* 404:731–747.
46. Villarroya, M. e. a. 1999. Voltage inactivation of  $\text{Ca}^{2+}$  entry and secretion associated with N- and P/Q-type but not L-type  $\text{Ca}^{2+}$  channels of bovine chromaffin cells. *J. Physiol.* 516:421–432.
47. Hofer, G., K. Hohenthanner, W. Baumgartner, K. Groschner, N. Klugbauer, F. Hofmann, and C. Romanin. 1997. Intracellular  $\text{Ca}^{2+}$  inactivates L-type  $\text{Ca}^{2+}$  channels with a Hill coefficient of 1 and an inhibition constant of  $4\mu\text{M}$  by reducing channel's open probability. *Biophys. J.* 73:1857–1865.

48. Atwater, I., B. Ribalet, and E. Rojas. 1978. Cyclic changes in potential and resistance of the beta-cell membrane induced by glucose in islets of Langerhans from mouse. *J. Physiol.* 278:117–139.
49. Solimena, M. 2006. private communication.
50. Straub, S., G. Shanmugan, and G. Sharp. 2004. Stimulation of Insulin Release by Glucose Is ssociated With an Increase in the Number of Docked Granules in the "s-Cells of Rat Pancreatic Islets. *Diabetes.* 53:3179–3183.
51. Gentet, L., G. Stuart, and J. Clements. 2000. Direct Measurement of Specific Membrane Capacitance in Neurons. *Biophys. J.* 79:314–320.
52. Goepel, S., Q. Zhang, L. Eliasson, X. Ma, J. Galvanovskis, T. Kanno, A. Salehi, and P. Rorsman. 2004. Capacitance measurements of exocytosis in mouse pancreatic alpha-, beta- and delta-cells within intact islets of Langerhans. *J. Physiol.* 556:711–726.
53. Smith, P. 1988. Electrophysiology of B-cells from pancreatic islets of Langerhans. Ph.D thesis. University of East Anglia.
54. Wasserman, W., and L. Smith. 1981. Calmodulin triggers the resumption of meiosis in amphibian oocytes. *J. Cell. Biol.* 89:389–394.

## 5 Supplementary material

### 5.1 Conductivity of membrane proteins

The (electrical charge) currents entering Eq. 1 and Eq. 4 are themselves dynamic quantities. Channels are gated in dependence on the membrane potential, on the presence of ATP, and on glucose- and ion- concentration. The resulting current depends on the electrochemical gradient over the membrane. So every membrane protein has its own characteristics and the conductivity of passive or active ion flow depends on different other parameters. In the following the different membrane proteins (as listed in Tab. 1) and their gating/activity properties are described in more

Na,K	sodium-potassium exchanger (Na <sup>+</sup> outwards, K <sup>+</sup> inwards)
Na,V	voltage-gated sodium channels
NCX	sodium-calcium exchanger (Na <sup>+</sup> inwards, Ca <sup>2+</sup> outwards)
PMCA	Plasma-membrane-calcium-ATPase (Ca <sup>2+</sup> outwards)
K,ATP	ATP-driven (and glucose-dependent) potassium channels
K,V	voltage-gated potassium channels (also called delayed rectifier)
K,Ca	voltage- and calcium-gated potassium channel
Ca,L	L-type voltage-dependent calcium channels
Ca,T	T-type voltage-dependent calcium channels

Table 1: **Acronyms of transmembrane proteins:** Acronyms for the different plasma membrane proteins contributing to ion flow through the membrane are defined. *Inwards* and *outwards* specifies in which direction the ion flows, i.e. in or out of the cell.

detail. Currents through pores are generally approximated by a linear voltage-current relation, which infers currents proportional to the electrical potential gradient (terms with  $V - \bar{V}$  with  $\bar{V}$  the reversal potential of the ion under consideration). For some channels and for extreme depolarisations there might be deviations from this approximation.

The activation dynamics of active carrier proteins relies on the Hill-function

$$H(x, x_h, n) = \frac{x^n}{x^n + x_h^n} \quad , \quad (6)$$

which can be derived from chemical kinetics.  $x$  denotes some concentration,  $x_h$  is the corresponding concentration of half activation, and  $n$  is the Hill-coefficient. Large  $n$  make the switch between inactive and active states steeper.

The asymptotic state of activation and inactivation is described by two functions of sigmoidal shape

$$\begin{aligned} \sigma_{\text{act}}(x, x_h, \kappa) &= \frac{1}{1 + \exp\{(x_h - x)/\kappa\}} \\ \sigma_{\text{inact}}(x, x_h, \lambda) &= \frac{1}{1 + \exp\{(x - x_h)/\lambda\}} \quad , \end{aligned} \quad (7)$$

Such sigmoidal functions are frequently used in literature and the parameters of these functions are determined in experiments.  $x_h$  is the concentration of half-maximum value and  $\kappa$  and  $\lambda$



regulate the activation and inactivation steepness, respectively. Inactivation is a property of ion channels which will be handled in complete analogy to activation. In a first approximation ATPases driving ions against their chemical gradient are inactivated. Only the channels Na,V; K,V; K,Ca; Ca,L; and Ca,T (see Tab. 3 and 4) are subject to inactivation.

### 5.1.1 The sodium-potassium exchanger Na,K

The sodium potassium exchanger transports sodium out of the cell and potassium into the cell. Both transport processes are against the chemical gradient, so that this process has to consume energy which is provided by ATP. The current is modelled as

$$I_{\text{Na,K}} = \overline{I_{\text{Na,K}}} (1 - H(K, K_{\text{Na,K}}, n_{\text{Na,K}})) H(N, \tilde{K}_{\text{Na,K}}, \tilde{n}_{\text{Na,K}}) \quad , \quad (8)$$

where  $\overline{I_{\text{Na,K}}}$  denotes the maximum current. The quantities used for the Hill-function are explained after Eq. 6. The first term describes a decreasing activity with increasing potassium concentration. The second one an increasing activity with increasing sodium concentration (see (22)). This approach follows approximations frequently adopted in other models: The adaption of Na,K-activity to sodium and potassium levels is assumed quick such that the steady state approximation is justified. A direct impact of glucose on Na,K-activity in  $\beta$ -cells (23) and a voltage-dependence of Na,K-activity (22) is neglected. As ATP-dynamics are not modelled, the ATP-level does not influence Na,K-activity.

**Activation dynamics:** The used parameters follow those found in (22) to fit experimental activation dynamics. Good agreement is found with  $n_{\text{Na,K}} = 2$  and  $K_{\text{Na,K}} = 33mM$  as well as  $\tilde{n}_{\text{Na,K}} = 2$  and  $\tilde{K}_{\text{Na,K}} = 20mM$  for dependence on potassium and sodium, respectively.

**Stoichiometry:** The stoichiometry of the exchanger is 3:2, thus 3 sodium ions are exchanged against 2 potassium ions entering the cell, i.e.  $\alpha_{\text{Na,K}} = 1.5$  in Eqs. 1 and 4. As both ions have the valence 1 this corresponds to 1 positive charges leaving the cell for 2 potassium ions entering the cell. Thus  $\overline{I_{\text{Na,K}}} > 0$  enters the different equation with different factors: +1 for  $V$  Eq. 4, -2 for  $K$ , and +3 for  $N$  Eq. 1.

**Turnover rate:** The turn over rate of one ATPase measured as the consumption of ATP-molecules per second is  $\overline{I_{\text{Na,K}}} = 200ATP/sec \approx 0.00003pA$  in canine cardiac neurons (24), where the last equality assumes one exchange of 3 sodium and 2 potassium per ATP.

### 5.1.2 The voltage gated sodium channel Na,V

The voltage gated sodium channel opens when the cell is depolarised. The sodium ions then follow their electrochemical gradient to flow into the cell. The current is therefore composed of two factors, one describing the open-probability of the channel, the other describing the flow through the open channel:

$$I_{\text{Na,V}} = h_{\text{Na,V}} g_{\text{Na,V}} \overline{g_{\text{Na,V}}} (V - \overline{V_{\text{Na}}}) \quad . \quad (9)$$

$\overline{V_{\text{Na}}}$  is the sodium reversal potential, and  $\overline{g_{\text{Na,V}}}$  is the maximum conductivity. The open and inactivation probabilities  $g, h_{\text{Na,V}}$  are assumed to exponentially reach their asymptotic values

and, thus, follow the kinetic equations

$$\begin{aligned}\frac{dg_{\text{Na},V}}{dt} &= \frac{\sigma_{\text{act}}(V, V_{\text{Na},V}, \kappa_{\text{Na},V}) - g_{\text{Na},V}}{\tau_{\text{Na},V}} \\ \frac{dh_{\text{Na},V}}{dt} &= \frac{\sigma_{\text{inact}}(V, W_{\text{Na},V}, \lambda_{\text{Na},V}) - h_{\text{Na},V}}{\theta_{\text{Na},V}}.\end{aligned}\quad (10)$$

The parameters are explained after Eq. 7. It is  $\tau_{\text{Na},V}$  that defines the time constant of adaptation of the sodium channel (the speed of conformity change) in response to a changed membrane potential, while  $\theta_{\text{Na},V}$  determines the time scale of channel inactivation.

**Conductivity:** The single channel conductivity of the voltage-gated sodium channel is  $\overline{g_{\text{Na},V}} = 14pS$  as found in the squid axon (25). This value is consistent with findings in other systems. Taking the results in mice  $\beta$ -cells (26), one has a single channel current of  $1pA$  at  $-30mV$  which (using  $V_{\text{Na}} = 80mV$ ) corresponds to  $9pS$ .

**Activation properties:** Activation is observed between  $-60mV$  and  $-10mV$  (26). Thus, a realistic approximation for the activation dynamics is  $V_{\text{Na},V} \approx -35mV$  and  $\kappa_{\text{Na},V} \approx 8mV$ .

**Inactivation properties:** The role of voltage-gated sodium channels in insulin secretion and in membrane depolarisation is controversial. Depending on species, the half-maximal inactivation is found at  $-109mV$  in mouse  $\beta$ -cells (26) (where  $2.6mM$  calcium were used, and at less calcium the inactivation point was shifted to even lower voltage) and total inactivation is found at  $-40mV$  (27, 28). Thus, one may estimate  $W_{\text{Na},V} \approx -100mV$  with a steepness of  $\lambda_{\text{Na},V} \approx 20mV$  (in order to get the observed total suppression of inactivation at  $-150mV$ , and total inactivation at  $-40mV$ ). This very low half inactivation potential is fully consistent with measurement in islet- $\beta$ -cells (19) and suggests an unprobable major role in the electrophysiology of  $\beta$ -cells (26), which is not confirmed in the present simulations.

**Time scales:** According to the sodium currents as observed in squid giant axons and to the classical description by Hodgkin-Huxley the time constant of activation depends on the membrane potential (11). This is represented by

$$\tau_{\text{Na},V} = \frac{c}{\exp\{(V - V_0)/a\} + \exp\{(V_0 - V)/b\}} \quad (11)$$

with  $c = 11.5ms$ ,  $a = 40mV$ ,  $b = 50mV$ , and  $V_0 = -70mV$ . Similar  $\tau_{\text{Na},V}$  are found in islet- $\beta$ -cells (19). Note that the same simulation results are found with the constant average value of  $\tau_{\text{Na},V} = 3ms$ . Inactivation happens on a time scale of  $\theta_{\text{Na},V} = 4.6ms$  which was found by two pulse experiments (11).

**Calcium permeability of sodium channels:** Sodium channels in neurons are in general permeable for calcium ions. Therefore, Na,V-channels are explicitly blocked with TTX in experiments to investigate the opening dynamics of voltage-gated calcium channels in order to separate these from the currents through sodium channels (see e.g. (29)). Calcium permeability of Na,V is not considered in the present approach.

### 5.1.3 The sodium-calcium exchanger NCX

The sodium-calcium exchanger takes advantage of the electrochemical gradient of sodium (pushing sodium into the cell) to transport calcium ions against its electrochemical gradient. This exchanger is important to reestablish the resting state calcium concentration after an excitable calcium influx into the cell. As in the case of the sodium-potassium exchanger a fast adaption of the activity to the calcium concentration is assumed. The current is derived from a corresponding Hill-function:

$$I_{\text{NCX}} = \overline{I_{\text{NCX}}} H(C, C_{\text{NCX}}, n_{\text{NCX}}) \quad . \quad (12)$$

Typical values for the single membrane protein parameters can be found in (10):  $\overline{I_{\text{NCX}}} = -0.0005 \text{ pA}$  (30) and  $C_{\text{NCX}} = 0.0022 \text{ mM}$  (31). The Hill coefficient is assumed to be  $n_{\text{NCX}} = 1$ . This is justified by the linear relationship between the observed current and the calcium concentration as observed for low calcium concentrations in cardiac cells (32). However, the NCX-Hill-coefficient is controversial (2, 33).

**Stoichiometry:** The stoichiometry of NCX is 3:1, i.e.  $\alpha_{\text{NCX}} = 3$  in most tissues (31), thus three sodium ions have to enter the cell in order to expel one calcium ion. The net current of NCX is one positive charge getting into the cell for every expelled calcium ion. This infers that  $\overline{I_{\text{NCX}}} < 0$ .  $I_{\text{NCX}}$  enters the different equations with factor  $+1$  for the equation for the membrane potential Eq. 4, a factor  $-1$  in the calcium equation, and a factor  $\alpha_{\text{NCX}}$  in the sodium equation Eq. 1.

**Impact of sodium-concentration:** Note that in the present description Eq. 12 the sodium concentration does not enter, even though NCX activity also depends on the sodium concentration gradient. Even though the sodium dynamics is modelled, it is assumed that the sodium concentration gradient is approximately constant. This turns out to be a reasonable approximation. In contrast, to neurons, in  $\beta$ -cells peaks in the potential are dominantly generated by calcium and not by sodium.

**Impact of ATP:** A dependence of the NCX activity on intracellular ATP concentration has been observed (34). This might be included in improved versions of this model that treat ATP dynamically.

### 5.1.4 PMCA

PMCA is an ATP-driven calcium pump extruding calcium from the cell to the extracellular medium, which has been characterised in  $\beta$ -cells (35). In a first attempt the dependence on the ATP concentration is ignored and the ATP-concentration is assumed to be large enough to make the pump work optimally. Then the activity is mainly dependent on the calcium concentration in the cell. A suitable modelling approach is

$$I_{\text{PMCA}} = \overline{I_{\text{PMCA}}} H(C, C_{\text{PMCA}}, n_{\text{PMCA}}) \quad . \quad (13)$$

The maximum current  $\overline{I_{\text{PMCA}}}$  is positive, as it carries calcium out of the cell. A delayed activation of PMCA by increased calcium has been observed (36) which is neglected in the present model (using the steady state approximation).

**Stoichiometry:** One calcium ion is transported per used ATP molecule leading to the stoichiometry of  $\alpha_{\text{PMCA}} = 1$  (37). This is surprising in view of the Hill-coefficient which was determined to be  $n_{\text{PMCA}} = 2$  (38), which would suggest a corresponding stoichiometry (see also the discussion in (39)).

**Turnover rate:** The turnover rate of single PMCA is in the order of 30 Hertz (30) corresponding to an activity rate of  $k_a = 0.03/ms$  (this value was also used in (3)). This turnover rate can be translated into an electrical current: Every pumping event corresponds to a flow of 2 electrical charges  $e$  leading to  $\overline{I}_{\text{PMCA}} = z_{\text{Ca}} e k_a = 60 \cdot 1.6 \cdot 10^{-19} C/s \approx 10^{-17} A = 10^{-5} pA$ .

**Half activation concentration:** Typical values for the half activation calcium concentration are  $C_{\text{PMCA}} = 0.1 \mu M$  (see e.g. (40) Figure 3). Note that the values of half activation are found to depend on the calmodulin concentration and the isoform under consideration (40) which is neglected in the present approach. The 4b-isoform has a slightly larger half activation concentration of  $0.16 \mu M$  (40).

**ATP consumption:** If modelling ATP concentration dynamics PMCA has to be considered as a major consumer of ATP. Note that up to 40% of the ATP consumed to pump calcium out of the cell is used by SERCA-ATPase, thus, not in the plasma membrane but at the endoplasmatic reticulum (14).

### 5.1.5 ATP-driven potassium channel K,ATP

The ATP-driven potassium-selective channel (also called G-channel (8)) uses ATP to open the channel and to release potassium from the cell. This process is, however, also regulated by the presence of glucose which is a source for ATP-metabolism in mitochondria. At normal glucose levels the channel has a resting state open probability, which is counteracted by the activity of the sodium-potassium exchanger. Note that about 50% of the potassium current is mediated by K,ATP channels (7). At increased levels of glucose the opening of this channel is inhibited. The single protein current is modeled by (see also Eq. 9):

$$I_{\text{K,ATP}} = (1 - g_{\text{K,ATP}}) \overline{g_{\text{K,ATP}}} (V - \overline{V}_{\text{K}}) \quad , \quad (14)$$

with

$$\frac{dg_{\text{K,ATP}}}{dt} = \frac{\sigma_{\text{act}}(\gamma, \gamma_{\text{K,ATP}}, \kappa_{\text{K,ATP}}) - g_{\text{K,ATP}}}{\tau_{\text{K,ATP}}} \quad . \quad (15)$$

Here,  $\gamma$  is the glucose concentration. All other parameters are in full analogy to the voltage-gated sodium channel Na,V.

**Ohmic conductivity and calcium dependence:** In the resting state the current is dominantly flowing through this channel (28) which explains why the resting potential is near of the potassium reversal potential. It is controversial whether the current-voltage relation is ohmic ( (28) versus (8, 9)). The latter authors show an ohmic relation in the relevant range of membrane potentials which justifies the present model (see (9) Fig. 2, (8) Fig. 1b). The opening frequency is observed to depend neither on the membrane potential nor on the calcium level (9, 28) which justifies the present approximation Eqs. 14 and 15.

**Conductivity:** The conductivity of single open channels is in the order of  $50pS$  for relevant membrane potentials (8) where also the dependence on the glucose level was investigated. This is consistent with the finding that with increasing depolarisation of the cell increasing outflow of potassium is observed with a single channel conductivity of  $\overline{g_{K,ATP}} = 54pS$  (9) (this value is used throughout all present simulations). An approximately linear current-voltage-relationship is found (9).

**Activation time scale:** The steady state approximation was used in two other models (4, 5). This points to a relatively short  $\tau_{K,ATP}$ . However, in an effective modelling approach (ignoring ATP concentrations) the time constant does not represent the time needed for the channel to adapt to a novel ATP-concentration but the time needed for the full metabolism process from glucose through ATP generation up to the changed open probability. The whole process from increased glucose levels up to exocytosis of insulin carrying granules take 1 minute (41), which defines an upper limit for  $\tau_{K,ATP}$ . Thus,  $\tau_{K,ATP}$  is chosen between this time and the time scale

**Glucose-driven deactivation:** As  $K_{ATP}$  provides the dominant part of potassium current in resting state it is assumed that the half-deactivation-concentration of  $K_{ATP}$  is around the resting level of glucose ( $\gamma_{K,ATP} = 1.2mM$ ). The steepness of the dependence on glucose is estimated as  $\kappa_{K,ATP} = 6mM$ .

**Modelling ATP-dynamics:** The present simulation might be improved by inclusion of ATP-dynamics as done in (2, 6). The functional relationship is well supported by experiment (13). This will be subject of further research.

**Other ATP-driven potassium channels** Other, novel, ATP-activated potassium channels have been observed in mice and humans, however, they differ in characteristics. They are still poorly defined but they are also believed to be involved in calcium oscillations. One additional channel found in human  $\beta$ -cells has a single-channel potassium conductivity of  $30pS$  (28).

### 5.1.6 The voltage-gated potassium channel $K_V$

The voltage gated potassium channel (also called delayed rectifier potassium channel) increases the potassium efflux from the cell once the cell is depolarised. The potassium ions follow their electrochemical gradient. The model for this channel is in complete analogy to the voltage-gated sodium channel Eq. 9:

$$I_{K,V} = h_{K,V} g_{K,V} \overline{g_{K,V}} (V - \overline{V_K}) \quad , \quad (16)$$

with

$$\begin{aligned} \frac{dg_{K,V}}{dt} &= \frac{\sigma_{act}(V, V_{K,V}, \kappa_{K,V}) - g_{K,V}}{\tau_{K,V}} \\ \frac{dh_{K,V}}{dt} &= \frac{\sigma_{inact}(V, W_{K,V}, \lambda_{K,V}) - h_{K,V}}{\theta_{K,V}} \quad . \end{aligned} \quad (17)$$

This is largely analogous to other models of  $\beta$ -cell bursting (2, 4, 5). However, the activation characteristics are not consistent in these models and inactivation is not considered ( (4) includes a different inactivating channel called  $I_{fast}$  therein). The present model is based on single protein properties exclusively derived from experiment.

**Conductivity:** Open channels have a single channel conductivity of  $\overline{g_{K,V}} = 10pS$  (28).

**Voltage-dependent activation:** K,V-channels in human  $\beta$ -cells were activated with a 400ms depolarisations to different membrane potentials (42). Then the membrane potential was reduced to -50mV and the current after this reset was monitored. The authors find a sigmoidal shape, centered at  $V_{K,V} = 1mV$  and width  $\kappa_{K,V} = 8.5mV$ .

**Time scale of activation:** The activation time constant is assumed to depend on the potential in (3) according to

$$\tau_{K,V} = \frac{c}{\exp\{(V - \overline{V_K})/a\} + \exp\{-(V - \overline{V_K})/b\}} \quad (18)$$

with  $c = 60ms$ ,  $\overline{V_K} = -75mV$ ,  $a = 65mV$ , and  $b = 20mV$ . This function is in agreement with experiments where the time constant was found to vary between 8 and 37ms (42).

**Slow channel inactivation:** For long depolarisations inactivation of the channels is observed. The characteristics are  $W_{K,V} = -25mV$  and width  $\lambda_{K,V} = 7.3mV$  (42). However, inactivation is not observed within 400ms so that we must conclude that  $\theta_{K,V} > 400ms$ . The value of 400ms is used in all simulations.

### 5.1.7 Calcium-gated potassium channel K,Ca

The calcium-gated potassium channel opens in dependence on the membrane potential and the intracellular calcium level. The dependence of the open probability on calcium is assumed to be in steady state and described by a Hill-function. Voltage-gating is described by an Ohm-like approach with dynamic gating (see also Eq. 9).

$$I_{K,Ca} = g_{K,Ca} \overline{g_{K,Ca}} (V - \overline{V_K}) H(C, C_{K,Ca}, n_{K,Ca}) \quad , \quad (19)$$

with

$$\frac{dg_{K,Ca}}{dt} = \frac{\sigma_{act}(V, V_{K,Ca}, \kappa_{K,Ca}) - g_{K,Ca}}{\tau_{K,Ca}} \quad (20)$$

All parameters are in analogy to other proteins described before. Other models that include detailed opening dynamics of K,Ca do not exist. The models (2,4,5) differ from the present one by very large Hill-coefficients (between 3 and 5) in a single Hill-function. As this is the first model of the K,Ca-opening dynamics it is explained in more detail.

**Ohmic conductivity:** The calcium-gated potassium channel is rapidly activated upon depolarisation and show a linear current-voltage relation (28). This justifies usage of an Ohm's law current.

**Conductivity:** The conductivity of single-channels  $\overline{g_{K,Ca}} = 220pS$  is rather large (28). This is also confirmed in rat muscle cells with values of up to 300pS depending on the temperature (20).

**Opening dynamics:** Experiments with rat muscle cells (20) show a dynamic activation in dependence on the membrane potential and of the calcium concentration (see also (28)). A sigmoidal opening probability is found for constant membrane potential in dependence of different



calcium concentrations (see (20) Fig. 6), but also for constant calcium with variable membrane potential (see (20) Fig. 8).

In a first approximation the opening dynamics is modelled by a product of a sigmoidal function and a Hill-function as shown in Eqs. 19 and 20. However, this approach turns out to be in contradiction to the data in (20). In order to reproduce these measurements more accurately, a dependence of the half activation calcium concentration  $C_{K,Ca}(V)$  on the voltage has to be assumed (see Figure 12):

$$\frac{dC_{K,Ca}}{dt} = \frac{C_{K,Ca}^{\infty}(V) - C_{K,Ca}}{\tau_{K,Ca}},$$

with  $C_{K,Ca}^{\infty}(V) = \exp\left\{\frac{a - V}{b}\right\}$  (21)

with  $a = 45mV$  and  $b = 30mV$ , and the same time delay than for the direct voltage-dependence (assuming related mechanisms). This is combined with a Hill-coefficient of  $n_{K,Ca} = 2$  and the

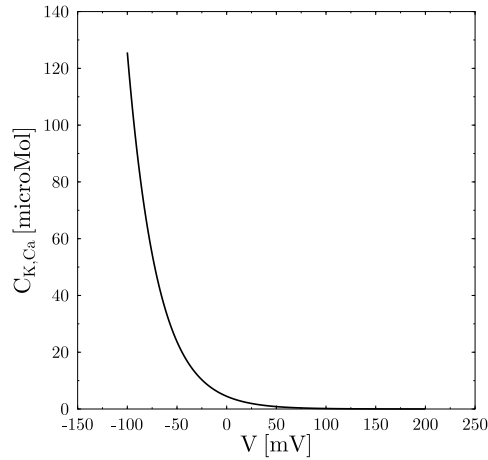


Figure 12: **Voltage-dependence of half activation:** The steady-state voltage-dynamics of the half activation calcium concentration  $C_{K,Ca}^{\infty}$  following Eq. 21 with  $a = 45mV$  and  $b = 30mV$ . Note that the dynamics is relevant at physiological membrane potentials.

sigmoidal function for the voltage-dependent activation with  $V_{K,Ca} = -40mV$  and  $\kappa_{K,Ca} = 25mV$ . We then get the result shown in Figure 13. A physiological interpretation of Eq. 21 is not obvious. Basically this equation says that less calcium is needed to reach the same level of activation when the cell is more depolarised. If the dependence of the opening probability on voltage and calcium level are supposed to correspond to two different molecular gating-mechanisms, then this equation says that either depolarisation acts on both mechanisms or the mechanism influenced by depolarisation acts back on the calcium-dependent mechanism. A concise interpretation is, however, lacking, and has to be clarified in further experiments.

**Inactivation:** Inactivation was only rarely observed. In rat muscle cells the channels remained open for several hundred milliseconds (20). Thus, inactivation of these channels is neglected in the model.



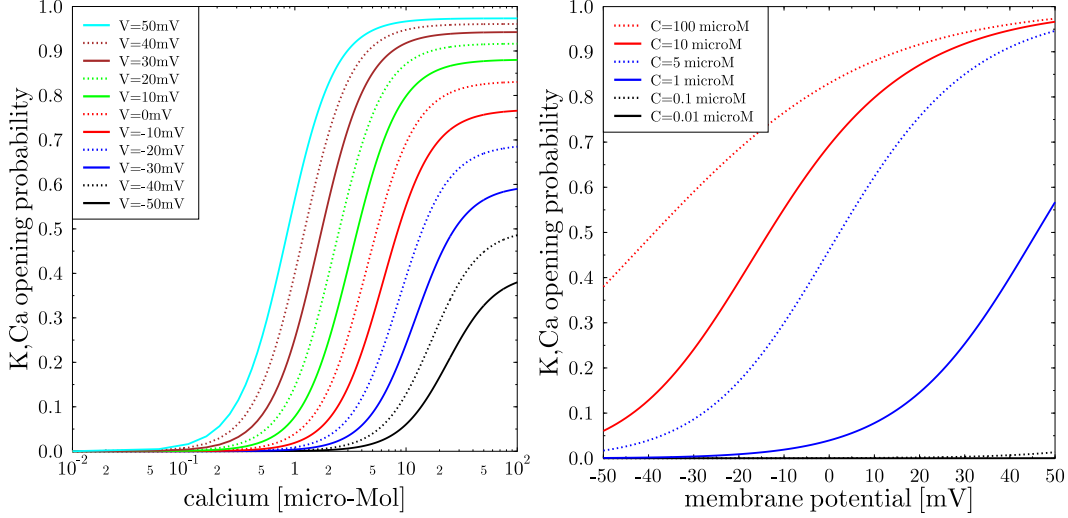


Figure 13: Opening probability of K,Ca using a product of a sigmoidal function (for  $V$ ) and a Hill-function (for calcium). The calcium concentration of half activation is assumed to depend on the membrane potential according to Eq. 21. The results are shown varying calcium (left panel) or the membrane potential (right panel). There is good agreement with the data in Fig. 8 (20). Parameters are  $a = 45mV$ ,  $b = 30mV$ ,  $n_{K,Ca} = 2$ ,  $V_{K,Ca} = -40mV$ , and  $\kappa_{K,Ca} = 25mV$ .

### 5.1.8 Voltage-gated calcium channels Ca,L/T

Voltage-gated calcium channels induce the inflow of calcium, following the electrochemical gradient of calcium, after an initial depolarisation of the cell. There are different subtypes of these channels which differ in their responsiveness. The dominant types in  $\beta$ -cells resemble L- and T-type channels (28) which can be classified as HVA- and LVA-channels, respectively. The equations for these channels are in analogy to the voltage-gated sodium channels Eq. 9

$$I_{Ca,L} = h_{Ca,L} (1 - H(C, C_{Ca,L}, n_{Ca,L})) g_{Ca,L} \overline{g_{Ca,L}} (V - \overline{V_{Ca}}) \quad , \quad (22)$$

with

$$\begin{aligned} \frac{dg_{Ca,L}}{dt} &= \frac{\sigma_{act}(V, V_{Ca,L}, \kappa_{Ca,L}) - g_{Ca,L}}{\tau_{Ca,L}} \\ \frac{dh_{Ca,L}}{dt} &= \frac{\sigma_{inact}(V, W_{Ca,L}, \lambda_{Ca,L}) - h_{Ca,L}}{\theta_{Ca,L}} \quad . \end{aligned} \quad (23)$$

For T-type channels all L's in the subscript have to be replaced by T. The term  $1 - H(\dots)$  appears only for L-type channels and has to be replaced by 1 for T-type. While HVA-channels were included in different ways in other models, LVA-channels were neglected in all other models. In the following a set of experiments providing opening characteristics of L- and T-type channels are summarised. The simulations will rely on the single protein characteristics as provided in (29).

**Single T-type (LVA) channel properties:** Open T-type channels show a single protein conductivity of  $\overline{g_{Ca,T}} \approx 10pS$  (29) (measured in dendrites of pyramidal neurons in CA1 hippocampus). They open already for membrane potentials near resting potential in the range of  $-70$  to  $-30mV$  with a half opening at  $-55mV$  (28). The threshold for opening was also measured in adrenal medulla endothelial cells (in whole-cell patch-mode) to be  $-50mV$  with  $V_{Ca,T} = -30mV$  (43) (this experiment uses calcium and not barium). The threshold value of  $-50mV$  was also found in (29) with  $V_{Ca,T} = -32mV$ . This consistently infers  $\kappa_{Ca,T} \approx 10mV$  in order to find low activity at the activation threshold. Indeed,  $\kappa_{Ca,T} = 7.0mV$  was found in (29). For inactivation  $W_{Ca,T} = -67mV$  and  $\lambda_{Ca,T} = 6.5mV$  are reported in (29). Activation happens on a time scale of  $\tau_{Ca,T} = 10ms$  while inactivation is rapid (28) but is slower with  $\theta_{Ca,T} = 18ms$  (43).

**Single L-type (HVA) channel activation:** Open L-type channels show a single protein conductivity of  $\overline{g_{Ca,L}} \approx 27pS$  (29), measured in dendrites of pyramidal neurons in CA1 hippocampus. In  $\beta$ -cells a single-channel conductivity of  $22pS$  was found (44). Activation is found between  $-40$  and  $0mV$  ( (28), (43) in a whole-endothelial cell measurement, and (45) in whole-cell measurements of mouse  $\beta$ -cells). The activation threshold is higher  $-20mV$  in CA1-pyramidal cells (29). The half maximal activation potential is  $V_{Ca,L} = -18mV$  (43) with a width of  $\kappa_{Ca,L} \approx 10mV$ . In CA1-pyramidal neurons measured with barium  $V_{Ca,L} = +9mV$  is found with  $\kappa_{Ca,L} = 6mV$  (29) (however, activation depends on the barium concentration in the patch). Channel characteristics have also been measured in  $\beta$ -cells with  $V_{Ca,L} = -3.8mV$  and  $\kappa_{Ca,L} = 8.4mV$  (44). The variability of whole-cell measurements of the currents is presumably related to different protein densities in different cell types rather than to different single-channel characteristics – see (43) and references in the discussion of L-type channels. Another ambiguity comes from the replacement of calcium by barium for technical reasons, which induces differences in the measured conductivity.

**No L-type inactivation observed:** Voltage-dependent inactivation is not observed for L-type ( (28), (45) in  $\beta$ -cells, (43) in endothelial cells, and (46) in bovine chromaffin cells (whole-cell measurement), (29) for CA1-pyramidal neurons). Thus,  $\tau_{Ca,L} > 1s$  is used. Note that the half inactivation potential and the steepness are irrelevant under these circumstances. Alternatively one could simply set  $h_{Ca,L} = 1$ .

However, there is an experiment showing inactivation of L-type channels in cardiac cells upon increased calcium levels (47). Inactivation was characterised by a Hill-function with Hill-coefficient  $n_{Ca,L} = 1$  (thus suggesting inactivation to be mediated by the binding of calcium ions to a single regulating site per  $Ca,L$ -protein) and half maximal inactivation at  $C_{Ca,L} = 4\mu M$ . This behaviour is included in this model for the first time by the additional factor  $1 - H(C, C_{Ca,L}, n_{Ca,L})$  in Eq. 22.

**Sodium conductivity:** In the same paper (44) it is also shown that the L-type calcium channels exhibit large conductivity of  $44pS$  for sodium, which is not considered in the simulations.

## 5.2 The leakage currents

The leakage currents in Eqs. 1 and 4 are calculated in the steady state approximation.

$$\begin{aligned}
-J_{\text{Na}} &= \rho_{\text{Na,V}} I_{\text{Na,V}}^{\text{ss}} + 2\rho_{\text{Na,K}} I_{\text{Na,K}}^{\text{ss}} \alpha_{\text{Na,K}} + \rho_{\text{NCX}} I_{\text{NCX}}^{\text{ss}} \alpha_{\text{NCX}} \\
-J_{\text{K}} &= \rho_{\text{K,ATP}} I_{\text{K,ATP}}^{\text{ss}} + \rho_{\text{K,V}} I_{\text{K,V}}^{\text{ss}} + \rho_{\text{K,Ca}} I_{\text{K,Ca}}^{\text{ss}} - 2\rho_{\text{Na,K}} I_{\text{Na,K}}^{\text{ss}} \\
-J_{\text{Ca}} &= \rho_{\text{Ca,L}} I_{\text{Ca,L}}^{\text{ss}} + \rho_{\text{Ca,T}} I_{\text{Ca,T}}^{\text{ss}} - z_{\text{Ca}} \rho_{\text{NCX}} I_{\text{NCX}}^{\text{ss}} + \rho_{\text{PMCA}} I_{\text{PMCA}}^{\text{ss}} \quad , \quad (24)
\end{aligned}$$

where the superscript ss denotes the steady state quantities. The calculated leakage currents guarantee that the cell exhibits a stable steady state and that the cell returns to its resting state after stimulation. In most alternative approaches the leakage currents were not considered (e.g. (3–5)).

The steady state currents are calculated from the steady state approximation of all kinetic equations for the open probabilities. These are evaluated on the basis of a set of properties in the resting state  $\{V_0, \gamma_0, N_0, K_0, C_0\}$ .

$$\begin{aligned}
I_{\text{Na,K}}^{\text{ss}} &= \overline{I_{\text{Na,K}}} (1 - H(K_0, K_{\text{Na,K}}, n_{\text{Na,K}})) \\
I_{\text{Na,V}}^{\text{ss}} &= \sigma_{\text{act}}(V_0, V_{\text{Na,V}}, \kappa_{\text{Na,V}}) \overline{g_{\text{Na,V}}} (V_0 - \overline{V_{\text{Na}}}) \\
I_{\text{NCX}}^{\text{ss}} &= \overline{I_{\text{NCX}}} H(C_0, C_{\text{NCX}}, n_{\text{NCX}}) \\
I_{\text{PMCA}}^{\text{ss}} &= \overline{I_{\text{PMCA}}} H(C_0, C_{\text{PMCA}}, n_{\text{PMCA}}) \\
I_{\text{K,ATP}}^{\text{ss}} &= (1 - \sigma_{\text{act}}(\gamma_0, \gamma_{\text{K,ATP}}, \kappa_{\text{K,ATP}})) \overline{g_{\text{K,ATP}}} (V_0 - \overline{V_{\text{K}}}) \\
I_{\text{K,V}}^{\text{ss}} &= \sigma_{\text{act}}(V_0, V_{\text{K,V}}, \kappa_{\text{K,V}}) \overline{g_{\text{K,V}}} (V_0 - \overline{V_{\text{K}}}) \\
I_{\text{K,Ca}}^{\text{ss}} &= \overline{g_{\text{K,Ca}}} (V_0 - \overline{V_{\text{K}}}) H(C_0, C_{\text{K,Ca}}(V_0), n_{\text{K,Ca}}) \sigma_{\text{act}}(V_0, V_{\text{K,Ca}}, \kappa_{\text{K,Ca}}) \\
I_{\text{Ca,L}}^{\text{ss}} &= \sigma_{\text{act}}(V_0, V_{\text{Ca,L}}, \kappa_{\text{Ca,L}}) \overline{g_{\text{Ca,L}}} (V_0 - \overline{V_{\text{Ca}}}) \\
I_{\text{Ca,T}}^{\text{ss}} &= \sigma_{\text{act}}(V_0, V_{\text{Ca,T}}, \kappa_{\text{Ca,T}}) \overline{g_{\text{Ca,T}}} (V_0 - \overline{V_{\text{Ca}}}) \quad , \quad (25)
\end{aligned}$$

where  $C_{\text{K,Ca}}(V_0)$  is calculated with Eq. 21. The intracellular resting concentrations of ions are used as given in Tab. 2:  $K_0 = 95\text{mM}$  (48),  $N_0 = 20\text{mM}$  (48),  $C_0 = 0.1\mu\text{M}$ .

## 5.3 Parameter lists

Variable	adapted from (3)	full model Figure 3	unit	reference
use leakage currents	no	yes	boolean	—
use inactivation	yes	yes	boolean	—
PMCA feedback to $V$	no	yes	boolean	—
cell radius $R_{\text{cell}}$	6.1	6.1	$\mu\text{m}$	(49, 50)
$C_{\text{m}}$	10	10	$fF/\mu\text{m}^2$	(51, 52)
$T$	310	310	$K$	—
$\gamma_0$	1	1	$mM$	(41)
$\gamma_{\text{stimulation}}$	none	10	$mM$	(18, 52)
$V_0$	-70	-70	$mV$	known
$K_0$	95	95	$mM$	(48)
$K_{\text{ext}}$	5.7	5.7	$mM$	Eq. 5: $\overline{V_K} = -75mV$
$N_0$	20	20	$mM$	(48): 20, (53): 36
$N_{\text{ext}}$	400	400	$mM$	Eq. 5: $\overline{V_{Na}} = 80mV$
$C_0$	0.1	0.1	$\mu M$	known
$C_{\text{ext}}$	1.5	1.5	$mM$	Eq. 5: $\overline{V_K} = 128mV$
use Nernst	no	yes	boolean	—
correct $\overline{V_{Ca}}$	no	78	$mV$	(11): $\overline{V_K} = 50mV$
calcium binding sites $c_0$	1.0	1.0	$mM$	(3): $0.3mM$ ; 1.0 implies $f_{Ca} \approx 0.1\%$
$K_c$	1	1	$\mu M$	(54)

Table 2: **General framework of the simulations:** The parameters as used in the full simulation in Figure 3 and the parameters needed to reproduce the model (3) are listed. Note that the latter differ from the values used in (3) and are adapted to today's knowledge. References given without comment support the value used in the full model.

Variable	adapted from (3)	full model Figure 3	unit	reference
$I_{Na,K}$	none	0.00003	$pA$	(24)
$K_{Na,K}$	none	33.3	$mM$	(22)
$n_{Na,K}$	none	2	#	(22)
$\bar{K}_{Na,K}$	none	20	$mM$	(22)
$\tilde{n}_{Na,K}$	none	2	#	(22)
$\alpha_{Na,K}$	none	1.5	Na/K	known
$\bar{g}_{K,ATP}$	none	54	$pS$	(8, 9, 28)
$\tau_{K,ATP}$	none	1	$s$	relatively slow
$\gamma_{K,ATP}$	none	1.2	$mM$	large current at resting state (7)
$\kappa_{K,ATP}$	none	6	$mM$	estimated
$\bar{g}_{K,V}$	10	10	$pS$	(28)
$\tau_{K,V}$	Eq. 18	Eq. 18	$s$	(42)
half max $\tau_{K,V}$	0.03	0.03	$s$	$8ms < \tau_{K,V} < 37ms$ (42)
$V_{K,V}$	-15	1.0	$mV$	(42)
$\kappa_{K,V}$	5.6	8.5	$mV$	(42)
$\theta_{K,V}$	none	400	$ms$	$(42) \leq 400ms$
$W_{K,V}$	none	-25	$mV$	(42)
$\lambda_{K,V}$	none	7.3	$mV$	(42)
$\bar{g}_{K,Ca}$	220	220	$pS$	(28), (20): $f(T)$
$C_{K,Ca}$	0.001	Eq. 21	$mM$	(20): $f(V)$
$n_{K,Ca}$	3	2	#	(20)
$\tau_{K,Ca}$	none	100	$ms$	estimated
$V_{K,Ca}$	none	-40	$mV$	(20)
$\kappa_{K,Ca}$	none	25	$mV$	(20)
$\bar{g}_{Na,V}$	none	14	$pS$	(25)
$\tau_{Na,V}$	none	Eq. 11	$s$	(11, 19)
$V_{Na,V}$	none	-35	$mV$	(26)
$\kappa_{Na,V}$	none	8.0	$mV$	(26)
$\theta_{Na,V}$	none	4.6	$ms$	(11)
$W_{Na,V}$	none	-100	$mV$	(19, 26, 28)
$\lambda_{Na,V}$	none	20	$mV$	(19, 26, 27)

**Table 3: Properties of single sodium and potassium conducting transmembrane proteins:** Properties of sodium and potassium conducting membrane proteins. References given without comment support the value used in the full model. A comment of the form  $f(X)$  denotes that the reference claim a dependence on the variable  $X$ .

Variable	adapted from (3)	full model Figure 3	unit	reference
$I_{\text{NCX}}$	none	-0.5	$fA$	(30)
$C_{\text{NCX}}$	none	1.8	$\mu M$	(31)
$n_{\text{NCX}}$	none	1	#	(10)
$\alpha_{\text{NCX}}$	none	3	Na/Ca	(31)
$I_{\text{PMCA}}$	0.01	0.01	$fA$	(30)
$C_{\text{PMCA}}$	1.8	0.1	$\mu M$	(40)
$n_{\text{PMCA}}$	2	2	#	(38)
$\alpha_{\text{PMCA}}$	1	1	Ca/ATP	(37)
$\bar{g}_{\text{Ca,L}}$	27	27	$pS$	(29, 44)
$\tau_{\text{Ca,L}}$	1	6	$ms$	(29): fast
$V_{\text{Ca,L}}$	0.0	0.0	$mV$	(29, 43, 44)
$\kappa_{\text{Ca,L}}$	12	12	$mV$	(28, 29, 44)
$\theta_{\text{Ca,L}}$	10	10	$s$	(29): no inact.
$W_{\text{Ca,L}}$	100	100	$mV$	(29): no inact.
$\lambda_{\text{Ca,L}}$	10	10	$mV$	(29): no inact.
$C_{\text{Ca,L}}$	none	4	$\mu M$	(47)
$n_{\text{Ca,L}}$	none	1	#	(47)
$\bar{g}_{\text{Ca,T}}$	none	10	$pS$	(29)
$\tau_{\text{Ca,T}}$	none	10	$ms$	(43)
$V_{\text{Ca,T}}$	none	-30	$mV$	(29)
$\kappa_{\text{Ca,T}}$	none	7.0	$mV$	(29)
$\theta_{\text{Ca,T}}$	none	18	$ms$	(43)
$W_{\text{Ca,T}}$	none	-67	$mV$	(29)
$\lambda_{\text{Ca,T}}$	none	6.5	$mV$	(29)

Table 4: **Properties of single calcium conducting transmembrane proteins:** Properties of calcium conducting transmembrane proteins. References given without comment support the value used in the full model.

Variable	adapted from (3)	full model Figure 3	unit
$\rho_{\text{K,ATP}}$	none	0.092	$/\mu m^2$
$\rho_{\text{K,V}}$	0.24	8.0	$/\mu m^2$
$\rho_{\text{K,Ca}}$	0.08	0.45	$/\mu m^2$
$\rho_{\text{Na,K}}$	none	2000	$/\mu m^2$
$\rho_{\text{Na,V}}$	none	1.15	$/\mu m^2$
$\rho_{\text{NCX}}$	none	7.5	$/\mu m^2$
$\rho_{\text{PMCA}}$	10000	1350	$/\mu m^2$
$\rho_{\text{Ca,L}}$	0.1	0.9	$/\mu m^2$
$\rho_{\text{Ca,T}}$	none	0.1	$/\mu m^2$

Table 5: **Densities of ion-conducting transmembrane proteins:** The densities of transmembrane proteins as used in the two simulation set-ups are listed. These parameters were used as fit parameters for the simulations. Thus, no references are given. Note that the large PMCA-density is a result of an unrealistic half activation calcium concentration used in (3) (see also Tab. 4).